

# Observational ozone data-sets over the global oceans and polar regions

## version 2024

Yugo Kanaya<sup>1</sup>, Roberto Sommariva<sup>2,3</sup>, Alfonso Saiz-Lopez<sup>4</sup>, Andrea Mazzeo<sup>5</sup>, Theodore K. Koenig<sup>6,47</sup>, Kaori Kawana<sup>1,7</sup>, James E. Johnson<sup>8,9</sup>, Aurélie Colomb<sup>10</sup>, Pierre Tulet<sup>11</sup>, Suzie Molloy<sup>12</sup>, Ian E. Galbally<sup>13</sup>,  
5 Rainer Volkamer<sup>14,15</sup>, Anoop Mahajan<sup>16</sup>, John W. Halfacre<sup>17</sup>, Paul B. Shepson<sup>18</sup>, Julia Schmale<sup>19</sup>, Hélène Angot<sup>20</sup>, Byron Blomquist<sup>15,21</sup>, Matthew D. Shupe<sup>21,15</sup>, Detlev Helmig<sup>22</sup>, Junsu Gil<sup>23</sup>, Meehye Lee<sup>23</sup>, Sean C. Coburn<sup>24</sup>, Ivan Ortega<sup>25</sup>, Gao Chen<sup>26</sup>, James Lee<sup>27,28</sup>, Kenneth C. Aikin<sup>15,29</sup>, David D. Parrish<sup>30</sup>, John S. Holloway<sup>15</sup>, Thomas B. Ryerson<sup>29</sup>, Ilana B. Pollack<sup>15, 29</sup>, Eric J. Williams<sup>15, 29</sup>, Brian M. Lerner<sup>31</sup>,  
10 Andrew J. Weinheimer<sup>25</sup>, Teresa Campos<sup>25</sup>, Frank M. Flocke<sup>25</sup>, J. Ryan Spackman<sup>32</sup>, Ilann Bourgeois<sup>33</sup>, Jeff Peischl<sup>29</sup>, Chelsea R. Thompson<sup>29</sup>, Ralf M. Staebler<sup>34</sup>, Amir A. Aliabadi<sup>35</sup>, Wanmin Gong<sup>34</sup>, Roeland Van Malderen<sup>36</sup>, Anne M. Thompson<sup>37</sup>, Ryan M. Stauffer<sup>37</sup>, Debra E. Kollonige<sup>37</sup>, Juan Carlos Gómez Martin<sup>38</sup>, Masatomo Fujiwara<sup>39</sup>, Katie Read<sup>28</sup>, Matthew Rowlinson<sup>28,17</sup>, Keiichi Sato<sup>40</sup>, Junichi Kurokawa<sup>40</sup>, Yoko Iwamoto<sup>41</sup>, Fumikazu Taketani<sup>1</sup>, Hisahiro Takashima<sup>42,1</sup>, Monica Navarro Comas<sup>43</sup>, Marios Panagi<sup>44</sup>, Martin G. Schultz<sup>45,46</sup>

15

<sup>1</sup>Japan Agency for Marine-Earth Science and Technology (JAMSTEC), Yokohama, Kanagawa 2360001, Japan

<sup>2</sup> School of Geography, Earth and Environmental Sciences, University of Birmingham, Birmingham, UK

<sup>3</sup> School of Chemistry, University of Leicester, Leicester, UK

<sup>4</sup>Department of Atmospheric Chemistry and Climate, Institute of Physical Chemistry Blas Cabrera, CSIC, Madrid 28006, Spain

<sup>5</sup> Lancaster Environment Centre, Lancaster University, Lancaster, UK

<sup>6</sup> State Key Joint Laboratory of Environmental Simulation and Pollution Control, BIC-ESAT and IJRC, College of Environmental Sciences and Engineering, Peking University, Beijing, China

<sup>7</sup> Now at Institute of Chemical Engineering Sciences, Foundation for Research and Technology–Hellas (FORTH/ICE-HT), Patras, 26504, Greece and School of Architecture, Civil and Environmental Engineering, École Polytechnique Fédérale de Lausanne (EPFL), Lausanne, 1015, Switzerland

<sup>8</sup> Cooperative Institute for Climate, Ocean, and Ecosystem Studies, University of Washington, Seattle, WA 98105, USA

<sup>9</sup> NOAA Pacific Marine Environmental Laboratory, Seattle, WA 98115, USA

<sup>10</sup> LAMP, Laboratoire de Météorologie Physique (UMR 6016 Université Clermont Auvergne, CNRS), Aubière, France

<sup>11</sup> LAERO, Laboratoire d'Aérologie (UMR 5560 CNRS, UT3, IRD), Toulouse, France

<sup>12</sup> Climate, Atmosphere & Ocean Interactions Program, Environment Research Unit, CSIRO, Aspendale, Victoria, Australia

<sup>13</sup> CSIRO Environment, Aspendale, Victoria, Australia

<sup>14</sup> Department of Chemistry, University of Colorado, Boulder, CO 80309-0215, USA

<sup>15</sup> Cooperative Institute for Research in Environmental Sciences (CIRES), University of Colorado Boulder, Boulder, CO, USA

<sup>16</sup> Centre for Climate Change Research, Indian Institute of Tropical Meteorology, Pashan, Pune 411008, India

<sup>17</sup> Wolfson Atmospheric Chemistry Laboratories, Department of Chemistry, University of York, York, YO31 7SH, UK

<sup>18</sup> School of Marine and Atmospheric Sciences, Stony Brook University, NY 11794-0701, USA

<sup>19</sup> Extreme Environments Research Laboratory, École Polytechnique Fédérale de Lausanne, EPFL Valais Wallis, Sion Switzerland

<sup>20</sup> Université Grenoble Alpes, CNRS, INRAE, IRD, Grenoble INP, IGE, Grenoble, France

<sup>21</sup> National Oceanic and Atmospheric Administration, Physical Sciences Laboratory, Boulder, CO, USA

<sup>22</sup> Boulder A.I.R. LLC, Boulder, Colorado, USA

<sup>23</sup> Department of Earth and Environmental Sciences, Korea University, Seoul, Republic of Korea

24 Precision Laser Diagnostics Laboratory, University of Colorado Boulder, Boulder, CO, USA

45 25 NSF National Center for Atmospheric Research, ACOM, Boulder, CO 80301, USA

26 NASA Langley Research Center, Hampton, VA 23681, USA

27 Department of Chemistry, University of York, York, UK

28 National Centre for Atmospheric Science, University of York, York, UK

29 NOAA Chemical Sciences Laboratory, Boulder, CO, USA

50 30 David.D.Parrish, LLC, Boulder CO. 80304 USA

31 Aerodyne Research, Inc., Billerica, MA, USA

32 NASA Ames Research Center, Moffett Field, CA 94035, USA

33 Université Savoie Mont Blanc, INRAE, CARRTEL, Thonon-Les-Bains F-74200, France

55 34 Air Quality Research Division, Science and Technology Branch, Environment and Climate Change Canada, Toronto, Ontario, M3H 5T4, Canada

35 University of Guelph, Guelph, ON, N1G 2W1, Canada

36 Royal Meteorological Institute of Belgium, Ringlaan 3, 1180 Uccle (Brussels), Belgium

37 NASA Goddard Space Flight Center, Greenbelt, MD 20771, USA

38 Instituto de Astrofisica de Andalucía, Consejo Superior de Investigaciones Científicas, 18008, Granada, Spain

60 39 Faculty of Environmental Earth Science, Hokkaido University, Sapporo 060-0810 Japan

40 Asia Center for Air Pollution Research, 1182 Sowa, Nishi-ku, Niigata, Niigata, 950-2144, Japan

41 Graduate School of Integrated Sciences for Life, Hiroshima University, Higashi-Hiroshima, Japan

42 Faculty of Science, Fukuoka University, Fukuoka, Japan

43 Atmospheric Research and Instrumentation Branch, National Institute for Aerospace Technology (INTA), Madrid, Spain

65 44 Climate and Atmosphere Research Center, The Cyprus Institute, 2121, Nicosia, Cyprus

45 Jülich Supercomputing Center, Forschungszentrum Jülich GmbH, 52425 Jülich, Germany

46 Department of Mathematics and Computer Science, University of Cologne, Germany

47 Now at Division of Environment and Sustainability, The Hong Kong University of Science and Technology, Hong Kong 999077, China

70 Correspondence to: Yugo Kanaya (yugo@jamstec.go.jp)

**Abstract.** Studying tropospheric ozone over the remote areas of the planet, such as the open oceans and the polar regions, is crucial to understand the role of ozone as a global climate forcer and regulator of atmospheric oxidative capacity. A focus on the pristine oceanic and polar regions complements the available land-based data-sets and provides insights into key photochemical and depositional loss processes that control the concentrations, spatio-temporal variability of ozone, and the physico-chemical mechanisms driving these patterns. However, an assessment of the role of ozone over the oceanic and polar regions has been hampered by a lack of comprehensive observational data-sets. Here, we present the first comprehensive collection of ozone data over the oceans and the polar regions. The overall data-set consists of 77 ship cruises/buoy-based observations and 48 aircraft-based campaigns. The data-set, consisting of more than 630,000 independent ozone measurement data points covering the period from 1977 to 2022 and an altitude range from the surface to 5000 m (with a focus on the lowest 2000 m), allows systematic analyses of the spatio-temporal distribution and long-term trends over the defined 11 ocean/polar regions. The data-sets from ships, buoys, and aircrafts are complemented with ozonesonde data from 29 launch sites or field campaigns, and by 21 non-polar and 17 polar ground-based stations data-sets. The datasets contained information on how long the observed air masses were isolated from land, as estimated by backward trajectories from the individual observation points. To extract observations representative of oceanic conditions, we recommend using a subset of the data with an isolation time

85 of 72 hours or longer, from the analysis with coincident radon observations. These filtered oceanic and polar data showed typically flat diurnal cycles at high latitudes, whereas at lower latitudes daytime decreases in ozone (11–16%) were observed. The ship/buoy- and aircraft-based data-sets presented here will supplement the land-based ones in the TOAR-II (Tropospheric Ozone Assessment Report Phase II) database to provide a fully global assessment of tropospheric ozone.

## 1. Introduction

90 As a short-lived species with an estimated lifetime of  $25.5 \pm 2.2$  days (Griffiths et al., 2021, Szopa et al., 2021), both global/hemispheric and regional/local aspects need to be emphasized in the assessment of tropospheric ozone. While the spatio-temporal variation over land is primarily important for assessing vegetation and health impacts, its behavior over the oceans is critical when assessing its climate impact as the third most important greenhouse gas (Forster et al., 2021). The role of ozone in maintaining the global oxidative capacity of the atmosphere through the production of the OH radical also requires 95 understanding on a global scale. The overall budget of tropospheric ozone is dominated by the photochemical production and loss terms, estimated at 4500–5000 and 3900–4500 Tg  $y^{-1}$ , respectively, rather than by the stratosphere-troposphere exchange (270–540 Tg  $y^{-1}$ ) or surface deposition (800–1000 Tg  $y^{-1}$ ) for decades around 2000 or 2010 (Griffiths et al., 2021; Young et al., 2018). The net ozone production mainly occurs over regions with NO<sub>x</sub> pollution and depends on the abundance of volatile organic compounds (VOCs). By contrast, the net loss conditions, which are driven by OH/HO<sub>2</sub> radical chemistry in a low NO<sub>x</sub> 100 environment and potentially also by understudied halogen chemistry, occur mostly over remote regions, including over the oceans (Galbally et al., 2000; Monks et al., 1998; Stone et al., 2018; Read et al., 2008; Dickerson et al., 1999; Boylan et al., 2015; Saiz-Lopez and von Glasow, 2012; Simpson et al., 2015). Another important loss term is from dry deposition on the ocean surface, which depends on the chemical composition of the surface seawater and its physical conditions (Helmig et al., 2012; Hardacre et al., 2015; Ganzeveld et al., 2009; Pound et al., 2020; Sarwar et al., 2016; Luhar et al., 2018; Barten et al., 105 2023; Chiu et al., 2024), and which has not been fully characterized. Therefore, there is a special need to study the ozone concentration levels, spatio-temporal variations, and underlying mechanisms that control ozone levels over the oceans. However, observational data of ozone over oceanic regions are much less abundant than those over the land, preventing a full 110 assessment. TOAR (Tropospheric Ozone Assessment Report) is an IGAC (International Global Atmospheric Chemistry project)-sponsored activity which aims to collect ozone observations in the troposphere. At the time of TOAR-I (Schulz et al., 2017), oceanic data were collected only from island-based surface monitoring observations and ozonesondes, with some satellite-based information, but the oceanic regions remained ~~with an apparent de~~void of data.

The polar regions ~~in the northern and southern hemispheres~~ are other pristine areas, with episodic ozone destruction in the polar sunrise season (Simpson et al 2007). During the ~~previous~~ International Polar Year 2007–2008, extensive studies on ozone were conducted and published (Atmospheric Chemistry and Physics (ACP) POLARCAT (Polar Study using Aircraft, Remote 115 Sensing, Surface Measurements and Models, of Climate, Chemistry, Aerosols, and Transport) special issue, 2015). An assessment report on short-lived climate forcers from the Arctic Council's Arctic Monitoring and Assessment Programme

(AMAP, 2021) and synthesis papers (Whaley et al., 2023, Law et al., 2023) have recently been produced, but comprehensive studies based on multi-platform observations are still lacking.

To improve the situation, a working group on ozone over the oceans and the polar regions (Oceans working group (WG)) has been formed within the TOAR-II activity to provide a comprehensive data-set, especially with ship-, buoy- and aircraft-based observations over the oceans, to allow a first assessment over the entire oceans and polar regions. In the past, studies on  $\Theta_3$  ozone over the oceans were conducted, using ship-based/aircraft-based  $\Theta_3$  ozone observations, but they were mostly based on observations from a single campaign or a series of related campaigns (e.g., Dickerson et al., 1999, Bourgeois et al., 2020) or at best from a collection of observations from a single nation/project (e.g., Lelieveld et al., 2004, Kanaya et al., 2019); here we aim to collect data from multiple nations, research groups, and campaigns to achieve a better global coverage, using the IGAC framework as a global research network (GRN) of Future Earth on which the TOAR activity is based. The resulting five datasets include observations from ships/buoys, aircraft, ozonesondes, ground-based coastal/island sites, and polar stations. This data paper primarily describes e-resulting two of these data-sets, which consist of 77 ship- or buoy-based observations and 48 aircraft observations over the global oceans and polar regions covering a period between 1977 and 2022, and are presented in this data paper. The altitude range covered by the data is from the surface to 5000 m, with a focus on the lowest 2000 m, as a major interest of the WG lies within the atmospheric boundary layer, where the interfacial interactions of the atmosphere with the ocean and snow/ice surfaces (even including biogeochemical processes), as well as the photochemistry, are of particular relevance. A third data-set contains ocean and polar ozonesonde data, mostly obtained from coastal/island sonde launching sites. The ozonesonde data were mainly provided by the HEGIFTOM (Harmonization and Evaluation of Ground-based Instruments for Free-Tropospheric Ozone Measurements) Focus Working Group of the TOAR-II activity and therefore include their data homogenization procedure (Van Malderen et al., 2025), but were further processed by the Oceans WG here. These three data-sets are complemented by two data-sets containing ground-based data from coastal/island sites and from polar stations, selected from the TOAR-II database (Schröder et al., 2024) with some additional field campaign sites. Satellite data are not included in this study because they are discussed elsewhere in the TOAR-II special issue (Gaudel et al., 2024; Pope et al., 2023) and because it is still difficult to resolve the commonly low ozone levels in the boundary layer over the oceans from satellite observations.

The result of this work enables integrated studies of the long-term and/or seasonal trends from ship-based observations and established coastal-site observations in the same region, for example at Cabo Verde, Kennaook-Cape Grim, Mace Head, and Trinidad Head (e.g., Parrish et al., 2009). To be suited for the ocean-focused studies, all five data-sets are complemented with information on how many hours each observed air mass was separated from land, derived from backward trajectories. Note that a full assessment of tropospheric ozone in the remote regions (oceans and polar) using these data-sets will be published separately (Sommariva et al., in preparation) as part of the TOAR-II series of assessment papers; here we focus on the data description, including its preparation and harmonization.

## 2 Data description

150 The overall geographical distribution of the collected ship-buoy data, aircraft-based data (up to 5000 m, but considering 0–  
2000 m altitude as a key part for the study of the boundary layer), and the locations of the selected ozonesonde/surface  
observation sites is shown in Fig. 1. The following subsections describe in detail each data-set. The data are divided into 11  
regions (2 polar and 9 oceanic). Following the recommendation of the TOAR-II Steering Committee (TOAR-II Steering  
Committee, 2023), the regions are broadly defined as follows: polar ( $\geq 60^{\circ}$  N and  $\geq 60^{\circ}$  S), mid-latitude (20–60° N  
155 and  $20^{\circ}$  S) and tropical ( $< 20^{\circ}$  N,  $< 20^{\circ}$  S). The boundaries are adjusted by 4 degrees or less to take into account  
geography or the position of the land masses (Fig. 1). The Pacific sector (from 100–115° E to 100–69° W, across the  
International Date Line) is subdivided into Northern (R1; 22–63° N), Tropical (R2; 20° S–22° N), and Southern (R3;  $20^{\circ}$   
 $60^{\circ}$  S) regions. The Indian Ocean (from 20–34° E to 100–115° E) is divided into Tropical (R4; 20° S–31° N) and Southern  
(R5;  $20^{\circ}$  S) regions. The eastern part of the Mediterranean Sea and the Black Sea (15–55° E, 31–59° N) are given a  
160 code R6 but we did not collect data because continental influences were generally unavoidable. The Atlantic sector (from 100–  
69° W to 15–20° E) is divided into Northern (R7; from 16–23° N to 62° N), Tropical (R8; 20° S–23° N, including the  
Caribbean), and Southern (R9;  $20^{\circ}$  S) regions. The Arctic region (R10) is defined as north of 59–63° N (depending  
on the longitude) and the Antarctic region (R11) as south of 60° S.

### 165 2.1 Ship/buoy data-set

A total of 208,291 of hourly averaged ozone concentration data were collected from 62 ship cruises (or aggregated  
cruises/legs) and from 15 buoy operations and archived in the file toar2\_oceans\_ship\_buoy\_data\_250203.csv, covering the  
period 1977–2022 (Table 1, Fig. 1). The data come from research groups in the USA, Japan, Australia, Germany, France,  
Switzerland, Spain, India, and the Republic of Korea. The instruments used are mainly research-grade ozone monitors based  
170 on UV absorption, with the exception of the DWD-MPI (Deutscher Wetterdienst - Max Planck Institute) data-set before 1996  
which used a wet chemical instrument using the potassium iodide (KI) method. The ship's exhaust plume could affect all of  
the cruise observations, depending on the relative wind directions with respect to the ship's funnel and the inlet position of the  
gas sampling tube. A fast response ozone monitor could easily detect such cases of pollution, as NO in the exhaust titrates the  
atmospheric ozone quickly. The buoy measurements do not have the risk of plume effect and therefore their hourly averages  
175 were constructed from the original 10-s raw data without filtering to preserve the real  $\text{O}_3$  reduction episodes over the  
Arctic region.

The ship datasets were processed as follows. First, minute data below (hourly mean) - (1  $\sigma$ ) were removed and then hourly  
averages were recalculated. The hourly data were removed if the variability of the valid minute data was greater than 10% of  
the hourly mean. The hourly data with minute data where the 1  $\sigma$  variability is >10% of the hourly mean are then removed.

180 This two-step filtering procedure is similar to Kanaya et al. (2019) and was found to be suitable to remove the ship's influence

in different cruise data-sets. Figure S1 shows a case of flagging and data removal from the time series of the R/V *Hakuho Maru* cruise KH18-6. Filtering was applied to cruises for which 1-minute based data were available, i.e., R/V Mirai cruises during 2012–2021(MR 12–21), *Hakuho Maru* KH-18-6, NAAMES1–4, ATOMIC, DYNAMO, WACS, VOCALS, NEAQS 2002, NEAQS 2004, TEXAQS 2006, ICEALOT, CalNex 2010, DRAKE2009, IN MAP-IO (SWINGS 2021, OP1 TAAF 2021, SCRATCH 2021, OP2 TAAF 2021, MAYOBS 2021, OP3 TAAF 2021, OP4 TAAF 2021; [www.mapio.re](http://www.mapio.re)), *Ka'imoana*, 17v01-05, 18v01-06, 08, 19v01-03, IIOE2, SOE9, and SOE11. The original data from MAGE92, RITS93, RITS94, ACE1, AEROSOLS99-INDOEX, ACE-Asia were on a 30-min basis, and ~~these from Malaspina, SAGA3, DWD MPI, YES AQ, MOSAiC were on an hourly basis. The 30-min data~~ were averaged to hourly. The original hourly data from Malaspina, SAGA3, DWD-MPI, YES-AQ, and MOSAiC were used as they were provided. We assumed that basic quality control has been performed (e.g., see Angot et al. (2022) for the MOSAiC data-set). The DWD-MPI data are a large compilation of 51 cruises with different research vessels (*Meteor*; *Polarstern*; *Walther Herwig*; *Anton Dohrn*; *Ymer*; *Academie*) collected by Deutscher Wetterdienst (DWD) in 1977–1996, 27 cruises with the container ship Berlin Express collected by Max Planck Institute (MPI) in 1995–2002, and one *Meteor* cruise conducted by MPI in 2002, with a clear note that the data have been screened for local influences of the research vessel itself and of nearby passing ships, and that data in and near harbours and in channels have been removed.

Some cruises included additional observations of pollution tracers, i.e., CO, NO, NO<sub>2</sub>, and condensation nuclei (CN) with diameters larger than 11–13 nm, and these data are archived together with ~~O<sub>3</sub>-ozone~~ (see Table 1 and Table S1 for the observation methods and uncertainties). However, the tracer observations did not cover the entire data-set and therefore could not be used uniformly for further systematic screening of air masses influenced by pollution arising from nearby land even if present. It is an essential requirement of oceanic ozone studies to be able to distinguish between air masses representing the remote ocean and those influenced by pollution from nearby land. Therefore, we calculated backward trajectories per hourly data-set to add the information of the "last contact with land (LCL, in the unit of hours ago)", as a semi-quantitative index indicating how long the air masses were isolated from a land region with potential pollution before the observations. The land mask data from NASA (NASA, 2019) with a resolution of 0.25° were used. The high-latitude regions ( $\geq 65^{\circ}$  N or  $\geq 69^{\circ}$  S) were not considered as "land", and the land mask was assumed only up to an altitude of 2500 m, as the pollution effect from land would be minimal at higher altitudes. Exceptions may include lifted plumes, such as those from biomass burning. The 2500-m threshold is tentative in an attempt to yield a criterion that is meaningful for the entire globe. It may be revisited after detailed analysis in the assessment. Backward trajectories were computed with the HYSPLIT version 4 model (Draxler and Rolph, 2013) using 6-hourly GDAS1 ( $1 \times 1^{\circ}$ ) meteorological fields after December 2004, or ~~the 6-hourly~~ NCEP/NCAR Reanalysis Project product (RP{YEAR}{MONTH}.bgl) files with 2.5° resolution for the earlier period. Harris et al. (2005) studied the uncertainty of the trajectories using NCEP/NCAR reanalysis. The starting altitude for ship/buoy observations was set to 500 m and the duration to 120 hours. The first point of land contact was marked to provide the LCL information. An LCL value of 120 h was assigned to the air masses if no land contact occurred for the entire period.

We defined a criterion of LCL  $\geq$  72 hours (hereafter referred to as LCL72) to identify marine air masses that have been  
215 minimally influenced by land. Figure 2 shows examples of the backward trajectories calculated for the MR19-03C cruise  
between Japan and the Arctic and for the RITS94 cruise from North to South America, respectively. The light blue and purple  
lines represent trajectories for marine and land-influencing air mass cases, respectively. The red lines indicate the cases where  
the observed  $\Theta_3$ -ozone mixing ratio was greater than 50 ppb (polluted).

The LCL72 criterion was evaluated using observed radon concentrations from ACE-1 (Whittlestone et al., 1998), ACE-Asia,  
220 ATOMIC, ICEALOT, NAAMES1–4, and WACS shipborne observations as a tracer of land contact (Fig. 3). Radon, emitted  
from land and lost with a half-life of 3.8 days (Zhang et al., 2021), is suitable for testing the performance of 120 h trajectories  
and then removing the cases affected by fresh pollution. The median and 3rd quartile Radon levels are diminished by almost  
two thirds when LCL increased from 10 to 80 hours, with a clear drop occurring between 60 and 80 hours since the last contact  
with land. This provides the basis for a 72 hours LCL threshold identifying marine air masses having little or no influence  
225 from land.

Although the discrimination between oceanic and land-influenced air masses is imperfect, largely due to the uncertainties in  
the trajectory calculations, the agreement between the LCL72 and the Radon  $<1000 \text{ mBq m}^{-3}$  criteria (during the campaigns  
for which this parameter was available) suggests that it is reasonable to apply the LCL72 flag to all the data treated in this  
230 study over the global oceans as the first filter against land influences. In subsequent studies on this oceanic ozone data-set,  
other filters of land influence can be developed and used to meet the requirements of the type of analysis being undertaken.  
For example, a more stringent criterion (Radon  $<100 \text{ mBq m}^{-3}$ ) was used to select baseline data at the Kennaook-Cape Grim  
station (Chambers et al., 2018). The data that met the LCL72 criterion covered 161,037 hours (77% of the original data-set).  
Note that the data with LCL less than 72 hours is kept in the data file, which may be useful for other purposes.

## 235 2.2 Aircraft data

Table 2 lists the 48 airborne campaigns included in the toar2\_oceans\_airborne\_data\_5000m\_250203.csv dataset. The land  
mask mentioned in Section 2.1 was used to extract the airborne observations over the oceans. The high latitude data ( $\geq 65$ – $90^\circ$   
N; or  $\geq 60$ – $90^\circ$  S) were not masked and were used directly. The original merge-type data files from aircraft observations had  
different time resolutions, from  $<10$  to 90 s; particularly for old missions only a coarse time resolution was available.  
240 Considering the temporal coverage and taking advantage of the relatively high temporal resolution of the more recent data, a  
variable temporal resolution in the range of 10–90 s was used. For campaigns where data with a higher temporal resolution  
(e.g., 1 Hz) were available, e.g., from FAAM measurements, the data were averaged over 10 s. A total of 424,005 and 252,086  
data records for the altitudes  $<5000$  m and  $<2000$  m, respectively, are included in the data-set, covering a period from 1987 to  
2020. The data ~~came originated~~ from the US, UK and Germany/Canada, and covered almost all global regions except for the  
245 R4 region (tropical Indian Ocean). Data for R5 (southern Indian Ocean) were sparse: only 62 points from the TRACE-A  
mission. The instruments used for the measurements of ozone are generally based on fast response, e.g., high sensitivity

chemiluminescence or UV absorption. Additional data on observations of pollutant tracers, i.e., CO, NO, and NO<sub>2</sub>, were archived together (Table S2). The backward trajectories were applied to each measurement point, similar to the ship/buoy-based data, with the starting altitude set to the GPS altitude of the aircraft or to 500 m when it was lower. The proportions of 250 the data meeting the LCL72 criterion were 74% and 63% for the <5000 m and <2000 m cases, respectively. This was partly affected by the assumed top altitude boundary of "land" at 2500 m. The bottom panel of Fig.1 shows the data meeting the LCL72 criterion and the altitude <2000 m.

### 2.3 Ozonesonde data

255 A total of 29 selected ozonesondes launch sites/campaigns are included in the toar2\_oceans\_ozonesondedata\_250203.csv dataset. The sites are listed in Table S3 and shown in Fig. 1. There are no data for regions R4 (Indian Ocean) and R9 (South Atlantic). As the availability of geopotential height information was considered a high priority in the creation of the dataset, data from earlier dates when this parameter was not available (e.g., Alert before 2000) were not included. Their inclusion could be a future task. The ozone mixing ratio was calculated from the atmospheric pressure and the ozone partial pressure data. To 260 reduce the data volume, one data point every 200 m (data closest to the top of each layer, e.g., near to 200 m, 400 m, etc.) was extracted up to the 5000 m altitude. The (1/e) ozone sensor response time (~30 s) gives the ozonesonde a vertical resolution of about 150 m for a typical balloon ascent rate (van Malderen et al., 2025). Most of the sites (24 out of 29) were taken from the homogenized HEGIFTOM dataset (Van Malderen et al., 2025) to ensure data quality. The selected launch sites are on islands or close to the coast. The other 5 data sources are from island and shipboard campaigns in the tropical Pacific, with the addition 265 of three data-sets in R11 (Antarctic region) from the World Ozone and Ultraviolet Radiation Data Centre (WOUDC) ozonesonde database to improve the coverage. The data are all from Electrochemical Concentration Cell (ECC) type ozonesondes. In total, 666,470 and 254,276 data points below 5000 and 2000 m altitude, respectively, were collected.

270 Backward trajectory calculations were only performed for selected heights (500, 1000, 1500, 2000, 3000, 4000, and 5000 m) to save ~~the~~ computational cost. The LCL information relative to the closest of the height points was used. The proportions of the data meeting the LCL72 criterion were 80% and 67%, for the full data-set (<5000 m altitude) and for the <2000 m data subset, respectively. As the launch site is usually on land, the latitude/longitude information from the backward trajectories at 0 and 1 h prior to launch was not included in the LCL calculation. Therefore, the potential influence of local air pollution in the vicinity of the launch site needs to be considered when using these data. For a further characterisation of air masses and screening, wind direction sector information (Table S3), constructed from the coordinates from the backward trajectory files 275 at 0 and 1 hour before launch, was added to the data-set.

### 2.4 Non-polar coastal sites data

The list of 21 non-polar coastal sites included in the toar2\_oceans\_coastsites\_250203.csv file is shown in Table S4, and their locations in Fig. 1: 16 sites are from the TOAR-II database (Schröder et al., 2024), 2 are from field campaigns, 2 are from

the EANET monitoring network, and 1 is from CSIRO. The sites were selected on the basis of the availability of high-quality  
280 data over long periods (typically for >10 years) and for the global coverage. However, no sites matching these criteria could be found for regions R4 and R5 (Indian Ocean). The Kennaook-Cape Grim dataset available on the TOAR-II database was not used, but rather another dataset provided by CSIRO. The latter was an updated version, extended through to the end of 2020, with the years 1982–2017 inclusive being fully QA/QC data on the WMO GAW/BiPM scale. The period 2018–2020 was in the final stages of QA/QC and the fully finalised dataset has subsequently been published on EBAS (EBAS, 2025).

285 Further information on the instruments and uncertainties for each site can be found in the TOAR-II database. Obviously, the  
~~incorrect data (i.e., zero or negative values) data~~ have been removed, resulting in a total of 3,650,267 hourly observations being included. The LCL information based on the backward trajectories is included. To save computational cost, only 6 hourly calculations were performed, and the result at the closest data timestamp was used. It should be noted that the risk of the influence from local air pollution is similar to that of the ozonesonde data-set. All sites, except Data from Trinidad Head, which  
290 can be screened using the local wind direction information (as shown in Table S3),~~can be considered, as only affected by air masses from essentially clean regions.~~

## 2.5 Polar sites data

The list of 17 polar coastal sites included in the toar2\_oceans\_polarsites\_250203.csv file is shown in Table S5 and Fig. 1.  
295 Except for Alert and Belgrano stations, where the data came from the Canadian data site and from National Institute for Aerospace Technology (INTA), respectively, the 15 data-sets are from the TOAR-II database. A total of 3,362,716 hourly observations were included. Similarly to the case of the non-polar coastal sites, the LCL information based on the backward trajectories is included. To save computational cost, only 6 hourly trajectory calculations were performed, and the result at the closest data timestamp was used.

## 300 3 Data overview

In this section, some basic data analysis and descriptive statistics of the collected data-sets is described, for informational purposes. Detailed discussion of the spatio-temporal distribution of tropospheric ozone and its trends over the oceans and polar regions will be presented in the assessment paper (Sommariva et al., in preparation).

### 305 3.1 Latitudinal, longitudinal, and vertical transects

Figure 4 shows the latitudinal and longitudinal cross sections of the ship/buoy data, after application of the LCL72 filter. The data are grouped into 10 degrees latitudinal and 20 degrees longitudinal bins. The median values in the southern hemisphere are in the range of 15.2–19.1 ppb, while those in the northern hemisphere are in the range of 20.5–34.0 ppb. As expected, a

maximum median value was found between 25–55° N, where the ozone is photochemically produced from precursors anthropogenically emitted over the continents and transported over long distances to the open oceans (Fig. 1, see also Kanaya et al., 2019). The longitudinal distribution has less variability, with median values in a narrow range of ca. 20–30 ppb. The high episodes (higher than 75 percentiles) are evident from 35–45° N and 120–140° E, suggesting that the effects of Asian pollution remain in the dataset, consistent with the discussion regarding the LCL72 filter.

Figure 5 shows the vertical profiles of the combined aircraft and ozonesonde data, after application of the LCL72 filter. The data are grouped into 250 m altitude bins. The general tendency is that ozone mixing ratios increase with height, except in R7 (Northern Atlantic), where the minimum median values occur in the 700–950 m layer, and in R8 (Tropical Atlantic), where ozone mixing ratios remain nearly constant from 1950 to 5000 m. The general tendency is that the ozone mixing ratio increases with height, except for R7 (Northern Atlantic), where the minimum median values occurred in the 700–950 m altitude layer. In the tropical Atlantic (R8) there is a constant ozone mixing ratio with height from 1950 to 5000 m, differing from the tropical Pacific (R2) and other regional profiles.

### 3.2 Seasonal coverage

Table S6 summarizes the number of observation days per region and season. For the ship/buoy data-set, the four seasons were relatively well sampled, but the frequencies were higher for boreal or austral summer than winter for mid- and high-latitude regions (R1, 3, 7, 9, 10, and 11). For the airborne data, coverage was less in summer than in winter over the Pacific, while the opposite was true for the Atlantic. The ozonesonde data-set appeared to have relatively uniform seasonal coverage, except that frequent observations were made during SON over the Antarctic (R11).

### 3.3 Ship/buoy-based median concentrations and diurnal variation patterns in individual regions (R1–R11)

Table 3 summarizes statistics of hourly data from the ship/buoy data-set (satisfying LCL72) to compare median concentrations across defined regions (R1–R11) and to investigate features of average diurnal profile (Fig. 6). First, the number of hourly data for individual regions ranged from 3446 (R4) to 61708 (R10), highlighting the advantage of having this large dataset in one place. For R10 (Arctic), 31549 and 7732 hours of data were from O-Buoy (autonomous, ice-tethered buoy) and MOSAiC (Multidisciplinary drifting Observatory for the Study of Arctic Climate) missions. The data-sets for the regions R7–R9 (Atlantic), with contributions from the DWD-MPI cruises, were larger than the Pacific (R1–R3). For all regions, the data are almost equally distributed over the time of day. The average diurnal profiles were calculated as follows: the local time was derived for each point was calculated from the time in by adjusting UTC with time based on longitude-shift, and then 25, 50, and 75 percentiles were calculated for each hourly bin per region.

The average of the 24-hourly medians showed variability across regions: For the northern midlatitudes, the Pacific and Atlantic were similar (32.9 and 31.6 ppb for R1 and R7, respectively). For the tropics, the Pacific (13.8 ppb, R2) was lower than the Indian Ocean (16.2 ppb, R4) and the Atlantic (20.0 ppb, R8). For the southern mid-latitudes, the values for the Pacific

and Indian Oceans were similar (20.1 and 19.7 ppb for R3 and R5, respectively), while the Atlantic was the lowest (15.4 ppb for R9). The R9 value is even lower than that of R8 and close to that of R11 (15.9 ppb, Antarctic). R10 (26.2 ppb) was slightly lower than R1 and R7 (northern mid-latitudes). While the mixing ratios over the tropics are frequently below 15 ppb, for 30%, 50%, and 59% over the Atlantic (R8), Indian (R4), and Pacific (R2) Oceans, respectively, but are very rarely near zero (<1% of observations are less than 3 ppb; Fig. 7). This is in marked contrast to the Arctic (R10) where a secondary distribution peak is found at around zero, while greater mean and median ozone levels are observed and only 18% of mixing ratios are less than 15 ppb. Roughly one third of these are ozone depletion events (ODEs) and 5.9% of total observations are below 3 ppb. This indicates that the mechanism(s) of Arctic ODEs is either inoperative or less efficient in the tropics.

As noted in Section 1, a unique feature of ozone in the marine boundary layer over the remote oceans is net photochemical loss. This must result in afternoon decreases in ozone levels. Indeed, flat diurnal patterns or daytime decreases are evident for the ship/buoy data in most regions (Fig. 6, Table 3). The diurnal profiles of the oceanic data suggest that the data-sets collected are representative of the marine atmosphere. More specifically, the three tropical regions R2, R4 and R8 show relatively large daytime decreases. The local time at which the minima were recorded was 15, 16 and 15 h for R2, R4 and R8, respectively (Table 3), while the maxima were recorded at night or in the morning. The different timings must be affected by dynamics and chemistry. The amplitude (maximum minus minimum) of the diurnal variation was 1.7, 2.6 and 2.3 ppb, or 12, 16 and 11% of the mean concentration for R2, R4 and R8, respectively. Previous studies from ship observations (Johnson et al., 1990; Thompson et al., 1993; Dickerson et al., 1999; Watanabe et al., 2005) and from coastal site observations (Oltmans, 1981; Nagao et al., 1999; Galbally et al., 2000; Read et al., 2008; Hu et al., 2010) have focused on diurnal variation with daytime decreases and reported amplitudes of 1–7.5 ppb (7–32% of average concentration levels). These studies are mainly from single sites/campaigns for short periods of time. Our dataset will be useful to investigate the characteristics of ozone diurnal variations more comprehensively and with statistical robustness. Contributions from various chemical pathways (e.g. HO<sub>x</sub> and halogen cycles) will be discussed by comparison with model simulations in the upcoming assessment paper. We also plan an in-depth analysis of our first observational findings, including the substantial reduction in the tropical Indian Ocean (R4), consistent with Dickerson et al. (1999), and the relatively early onset of daytime destruction for R8 and R2.

### 3.4 Consistency between the ground-based observations and the ozonesonde observations at the same sites

At 6 stations (Alert, Ny Ålesund, Trinidad Head, American Samoa, Syowa, and South Pole), both ground-based and ozonesonde observations were recorded. The consistency between the two data-sets was checked by comparing ozone measurements at ground level and the ozone sonde data at the lowest altitude (typically around 200 m). Figure 8 shows 3-year and 2-year comparisons at Alert and American Samoa, as an example. The agreement was found for cases of episodic  $\text{O}_3$  decreases in the Arctic and for temporal patterns of variation over days and seasons at both sites, demonstrating the internal consistency of the data-sets. Using the ground-based and ozonesonde observations in the Arctic (including Alert) for the year of 2015 as well as ship/buoy/aircraft observations, Gong et al. (2025) discuss the performance of two chemistry-transport models. Reasonable agreement was also found with scatterplots for all 6 sites (Fig. S2), with  $R^2$  values ranging from

0.64 to 0.95 and slopes of bivariate linear fits ranging from 0.94 to 1.11 when sonde values were plotted against surface  
375 observations made within one hour of each other. This analysis indicated the high quality of the two datasets.

## 4 Data availability

The data-sets described in this paper are available as five csv files containing all the corresponding metadata information. The files are named as follows:

1. toar2\_oceans\_ship\_buoy\_data\_250203.csv
2. toar2\_oceans\_airborne\_data\_5000m\_250203.csv
3. toar2\_oceans\_ozonesondedata\_250203.csv
4. toar2\_oceans\_coastalsites\_250203.csv
5. toar2\_oceans\_polarsites\_250203.csv

The files contain the key metadata information listed in Tables 1–5. The files are available at <https://doi.org/10.17596/0004044>  
385 (Kanaya et al., 2025).

## 5 Conclusions and outlook

Under the TOAR-II activity, the Oceans Working Group has, for the first time, collected and collated observational ozone data over the open oceans and polar regions on a global scale. When available, additional pollution tracers (CO, NO, NO<sub>2</sub>, CN) were also included. All these data-sets are stored in five data files classified by platform type, i.e. ship/buoy, aircraft,  
390 ozonesondes, non-polar coastal sites and polar sites. Here we describe the data-sets and the details of the pre-processing, filtering and flagging procedures, and show basic analyses of spatio-temporal extent, diurnal variation characteristics and internal consistency. Our focus was on the ship/buoy and aircraft observations, which contain a total of 208,291 and 424,005 records, respectively. The aircraft and ozonesonde data covered an altitude range from the surface to 5000 m, allowing a complete assessment of ozone over the oceans and polar regions with a focus on the atmospheric boundary layer (<2000 m).

All data-sets were supplemented with information on the number of hours that each observed air mass was separated from land, derived from backward trajectories. The selected criterion of 72 hours or more isolation from land, justified by the coincident radon observations for some selected data-sets, allowed the identification of marine air masses. Flat diurnal patterns or diurnal decreases were found after air mass selection, indicating that the collected data-sets are representative of the marine atmosphere.  
395 Over the tropics, the amplitude of the observed daytime decreases was 11–16%, with the largest decrease observed in the Indian Ocean.  
400

Although the observational data have been collected as widely as possible, they are still not sufficiently dense or homogeneous across the defined regions, particularly for the purpose of small trend detection (Chang et al., 2024). In order to interpret the data, the sampling bias needs to be assessed using atmospheric chemistry-transport numerical model simulations (e.g., Sekiya

et al., 2020). Even if the sampling bias is present, point-by-point comparisons with spatio-temporal matching model

405 simulations will be useful to study the key processes and mechanisms. Seasonality and long-term trends in the oceanic and polar ozone observations will be a focus of discussion in the forthcoming Assessment (Sommariva et al., in preparation).

## Appendix A. Acronyms and abbreviations

Table A1. List of acronyms and abbreviations.

Acronym	Definition
<u>ABLE-2B</u>	<u>Amazon Boundary Layer Experiment 2B</u>
<u>ABLE-3A/3B</u>	<u>Arctic Boundary Layer Experiment 3A/3B</u>
<u>ACCACIA</u>	<u>Aerosol-Cloud Coupling and Climate Interactions in the Arctic</u>
<u>ACE1</u>	<u>Aerosol Characterization Experiment 1</u>
<u>ACE-Asia</u>	<u>Aerosol Characterization Experiment – Asia</u>
<u>ACSYS</u>	<u>Atmospheric Chemistry and Climate of the Southern Indian Ocean</u>
<u>ACTIVATE</u>	<u>Aerosol Cloud meTeorology Interactions oVer the western ATLantic Experiment</u>
<u>AEROSOLS99-INDOEX</u>	<u>Indian Ocean Experiment 1999</u>
<u>ARCPAC</u>	<u>Aerosol, Radiation, and Cloud Processes affecting Arctic Climate</u>
<u>ARCTAS</u>	<u>Arctic Research of the Composition of the Troposphere from Aircraft and Satellites</u>
<u>ATom</u>	<u>Atmospheric Tomography Mission</u>
<u>ATOMIC</u>	<u>Atlantic Tradewind Ocean–Atmosphere Mesoscale Interaction Campaign</u>
BIPM	Bureau International des Poids et Mesures
<u>CalNex</u>	<u>California Nexus</u>
<u>CAST</u>	<u>Coordinated Airborne Studies in the Tropics</u>
<u>CITE</u>	<u>Chemical Instrumentation Test and Evaluation</u>
<u>CLARIFY</u>	<u>Cloud-Aerosol-Radiation Interactions and Forcing: Year 2017</u>
CN	Condensation Nuclei
<u>CONTRAST</u>	<u>Convective Transport of Active Species in the Tropics</u>
<u>CSIRO</u>	<u>Commonwealth Scientific and Industrial Research Organisation</u>
<u>DISCOVER-AQ</u>	<u>Deriving Information on Surface Conditions from Column and Vertically Resolved Observations Relevant to Air Quality</u>
<u>DRAKE</u>	<u>Drake Passage cruise</u>
DWD	Deutscher Wetterdienst
<u>DYNAMO</u>	<u>Dynamics of the Madden-Julian Oscillation</u>
ECC	electrochemical concentration cell
FAAM	Facility for Airborne Atmospheric Measurements
GAW	Global Atmosphere Watch Programme
GRN	Global Research Network
HEGIFTOM	Harmonization and Evaluation of Ground-based Instruments for Free-Tropospheric Ozone Measurements
<u>HIPPO</u>	<u>HIAPER Pole-to-Pole Observations</u>
<u>HURRICANE</u>	<u>Hurricane Field Campaign 2006</u>
HYSPLIT	HYbrid Single-Particle Lagrangian Integrated Trajectory
<u>ICEALOT</u>	<u>International Chemistry Experiment in the Arctic LOwer Troposphere</u>
IGAC	International Global Atmospheric Chemistry project
<u>IIOE2</u>	<u>Second International Indian Ocean Expedition</u>
<u>INTA</u>	<u>National Institute for Aerospace Technology</u>
<u>INTEX-B</u>	<u>Intercontinental Chemical Transport Experiment-B</u>

<a href="#">INTEX-NA</a>	<a href="#">Intercontinental Chemical Transport Experiment-North America</a>
<a href="#">ITCT</a>	<a href="#">Intercontinental Transport and Chemical Transformation</a>
<a href="#">ITOP</a>	<a href="#">Intercontinental Transport of Ozone and Precursors</a>
<a href="#">KORUS-AQ</a>	<a href="#">Korea-United States Air Quality Study</a>
LCL	Last Contact with Land
<a href="#">MAGE</a>	<a href="#">Marine Aerosol and Gas Exchange</a>
<a href="#">Malaspina</a>	<a href="#">Malaspina Circumnavigation Expedition</a>
<a href="#">MOSAiC</a>	<a href="#">Multidisciplinary drifting Observatory for the Study of Arctic Climate</a>
MPI	Max Planck Institute
<a href="#">NAAMES</a>	<a href="#">North Atlantic Aerosols and Marine Ecosystems Study</a>
<a href="#">NARE</a>	<a href="#">North Atlantic Regional Experiment</a>
NCEP	National Centers for Environmental Prediction
<a href="#">INTA</a>	<a href="#">National Institute for Aerospace Technology</a>
<a href="#">NEAQS</a>	<a href="#">New England Air Quality Study</a>
<a href="#">O-Buoy</a>	<a href="#">Autonomous, ice-tethered buoy</a>
ODEs	Ozone Depletion Events
<a href="#">PEM-Tropics</a>	<a href="#">Pacific Exploratory Mission-Tropics</a>
<a href="#">PEM-West</a>	<a href="#">Pacific Exploratory Mission-West</a>
<a href="#">POLARCAT</a>	<a href="#">Polar Study using Aircraft, Remote Sensing, Surface Measurements and Models, of Climate, Chemistry, Aerosols, and Transport</a>
<a href="#">RITS</a>	<a href="#">Research in the Tropics</a>
<a href="#">SAGA</a>	<a href="#">Surface Ocean Lower Atmosphere Study</a>
<a href="#">SEAC4RS</a>	<a href="#">Studies of Emissions and Atmospheric Composition, Clouds and Climate Coupling by Regional Surveys</a>
<a href="#">SOE</a>	<a href="#">Southern Ocean Expedition</a>
<a href="#">TAAF</a>	<a href="#">Terres australes et antarctiques francaises</a>
<a href="#">TEXAQS</a>	<a href="#">Texas Air Quality Study</a>
TOAR	Tropospheric Ozone Assessment Report
<a href="#">TORERO</a>	<a href="#">Tropical Ocean tRoposphere Exchange of Reactive halogen species and Oxygenated VOC</a>
<a href="#">TRACE-A</a>	<a href="#">Transport and Atmospheric Chemistry near the Equator-Atlantic</a>
<a href="#">TRACE-P</a>	<a href="#">Transport and Chemical Evolution over the Pacific</a>
<a href="#">VOCALS</a>	<a href="#">VAMOS Ocean-Cloud-Atmosphere-Land Study</a>
<a href="#">WACS</a>	<a href="#">Western Atlantic Climate Study</a>
WDCRG	World Data Centre for Reactive Gases
<a href="#">WG</a>	<a href="#">Working Group</a>
<a href="#">WINTERSTORMS</a>	<a href="#">Winter Storms Field Campaigns</a>
WOUDC	World Ozone and Ultraviolet Radiation Data Centre
<a href="#">YES-AQ</a>	<a href="#">YEllow Sea-Air Quality</a>

410

### Author contribution:

RS, ASL, and YK designed the study and led the data collection, assisted by TKK, AMaz, JEJ, SM, IEG, AMah, GC, WG, JCGM, KR, and MR. YK, FT, IY, HT, KK, JEJ, ASL, AC, PT, SM, IEG, RV, AMah, JS, HA, BB, MDS, DH, JG, ML, SCC, and IO carried out ship observations, collected data, and contributed to their quality control. JWH and PBS led the O-Buoy observations and contributed to their quality control. RV, TKK, JL, DDP, JSH, TBR, IBP, EJW, BML, AJW, TC, FMF, JRS, IB, JP, CRT, RMStae, and AAA conducted aircraft observations, collected data, and contributed to their quality control. RVM,

AMT, RMStau, DEK, JCGM, and MF performed ozonesonde observations, managed the data, and contributed to their quality control and homogenization. SM, IEG, WG, KS, JK, and MGS contributed to data collection from coastal/polar sites and analysis. MGS supervised the data collection and handling. MP contributed to data collection from surface sites. KCA and GC managed data and contributed to data curation including quality assurance. KK and TKK performed filtering of the ship-based data and figure generation. AMaz, TKK, KR, MR, IEG, RS, ASL and YK analyzed the dataset and prepared the figures and tables. YK drafted the manuscript and all the co-authors reviewed and contributed to revisions.

425 **Competing interests:**

The authors declare that they have no conflict of interest.

### Acknowledgements

We acknowledge NSF, UCAR/NCAR, NASA, NOAA (PMEL, CSD), ECCC, EANET, JAMSTEC, and NERC for funding 430 and data management. For R/V *Mirai* cruises, we gratefully acknowledge assistance from the Principal Investigators and staff members of all cruises and support from Global Ocean Development Inc. and Nippon Marine Enterprise, Ltd. Authors thanks the IN MAP-IO support team of the OSU-R and OMP for data from the *Marion Dufresne*. Peter Winkler, Marian de Reus, Jos Lelieveld, Jonathan Williams and Horst Fischer are acknowledged for the DWD-MPI dataset. We acknowledge the use of the CSIRO Marine National Facility (<https://ror.org/01mae9353>) in undertaking this research on R/V *Investigator*. The finalised 435 data will be available from the CSIRO Data Access Portal (DAP) with an accompanying DOI. Paty Matrai, Jan Bottenheim, and Bill Simpson are acknowledged for the O-Buoy data. Data collection as part of the international Multidisciplinary drifting Observatory for the Study of Arctic Climate (MOSAiC) expedition with the tag MOSAiC20192020, with activities supported by Polarstern expedition AWI\_PS122\_00. The observations during the MOSAiC expedition were funded by the US National Science Foundation (awards OPP 1807496, 1914781, and 1807163), the Swiss National Science Foundation (grant 440 200021\_188478), the Swiss Polar Institute (grant no. DIRCR-2018-004), the Department of Energy Atmospheric System Research Program (DE-SC0019251), and the US National Oceanic and Atmospheric Administration (NOAA) Physical Sciences Laboratory. A subset of data was provided by the Atmospheric Radiation Measurement (ARM) User Facility, a U.S. Department of Energy Office of Science User Facility managed by the Biological and Environmental Research Program. J.S. holds the Ingvar Kamprad chair for extreme environments research, sponsored by Ferring Pharmaceuticals. M.D.S. was 445 supported by the DOE (DE-SC0021341) and NOAA Cooperative Agreement NA22OAR4320151. I.B.P., J.P., C.R.T., I.B., and B.M.L. were supported in part by NOAA Cooperative Agreements NA17OAR4320101 and NA22OAR4320151. DH acknowledges funding by the US National Science Foundation, Interdisciplinary Biocomplexity in the Environment Program, Project No. BE-IDEA 0410058, and by a grant from NOAA's Climate and Global Change Program, NA07OAR4310168. The TORERO (Tropical Ocean tRoposphere Exchange of Reactive halogen species and Oxygenated VOC) and CONTRAST 450 (CONvective TRansport of Active Species in the Tropics) projects were funded by the National Science Foundation (AGS-1104104, AGS-1261740). The involvement of the NSF-sponsored Lower Atmospheric Observing Facilities, managed and

operated by the National Center for Atmospheric Research (NCAR) Earth Observing Laboratory (EOL) is acknowledged. The FAAM airborne data was obtained using the BAe-146-301 Atmospheric Research Aircraft [ARA] flown by Airtask Ltd and managed by FAAM Airborne Laboratory, jointly operated by UKRI and the University of Leeds. The HEGIFTOM homogenized ozonesonde data are from PIs David Tarasick, Peter von der Gathen, Nis Jepsen, Rigel Kivi, Bryan Johnson, and Terry Deshler. The WOUDC ozonesonde data are from the Finnish Meteorological Institute - National Meteorological Service of Argentina, Australian Bureau of Meteorology, and Japan Meteorological Agency (JMA) retrieved from the WOUDC site (<https://woudc.org/>). The ozonesonde sounding campaign from the research vessel *Shoyomaru* was conducted as part of the project Soundings of Ozone and Water in the Equatorial Region (SOWER) in collaboration with Japan Fisheries Agency.

455 Regarding the data from Kennaook-Cape Grim, Australian Bureau of Meteorology who own and manage the station, and CSIRO for producing the data-set are acknowledged. We gratefully acknowledge the NOAA Air Resources Laboratory (ARL) for providing the HYSPLIT transport model (<https://www.arl.noaa.gov/hysplit/>, last access: 23 November 2024). We acknowledge NDACC HEGIFTOM, SHADOZ data (<https://doi.org/10.57721/SHADOZ-V06>). The CONTRAST and TORERO data are from <https://doi.org/10.5065/D6PK0D6N> and <https://doi.org/10.26023/150P-D7CG-310>. This study was supported by the KAKENHI grant no. 21H04933), the ArCS (Arctic Challenge for Sustainability; grant no. JPMXD1300000000) and ArCS II (Grant Number JPMXD1420318865) of the Ministry of Education, Culture, Sports, Science, and Technology of Japan, the Specified Critical Technologies Research Promotion Grants from the Cabinet Office, Government of Japan, and by the Environmental Research and Technology Development Fund (ERTDF) from the Ministry of the Environment, Japan (JPMEERF20252001 and JPMEERF24S12200)

## 470 References

Abbatt, J. P. D., Leaitch, W. R., Aliabadi, A. A., Bertram, A. K., Blanchet, J.-P., Boivin-Riou, A., Bozem, H., Burkart, J., Chang, R. Y. W., Charette, J., Chaubey, J. P., Christensen, R. J., Cirisan, A., Collins, D. B., Croft, B., Dionne, J., Evans, G. J., Fletcher, C. G., Galí, M., Ghahreman, R., Girard, E., Gong, W., Gosselin, M., Gourdal, M., Hanna, S. J., Hayashida, H., Herber, A. B., Hesaraki, S., Hoor, P., Huang, L., Hussherr, R., Irish, V. E., Keita, S. A., Kodros, J. K., Köllner, F., Kolonjari, F., Kunkel, D., Ladino, L. A., Law, K., Levasseur, M., Libois, Q., Liggio, J., Lizotte, M., Macdonald, K. M., Mahmood, R., Martin, R. V., Mason, R. H., Miller, L. A., Moravek, A., Mortenson, E., Mungall, E. L., Murphy, J. G., Namazi, M., Norman, A.-L., O'Neill, N. T., Pierce, J. R., Russell, L. M., Schneider, J., Schulz, H., Sharma, S., Si, M., Staebler, R. M., Steiner, N. S., Thomas, J. L., von Salzen, K., Wentzell, J. J. B., Willis, M. D., Wentworth, G. R., Xu, J.-W., and Yakobi-Hancock, J. D.: Overview paper: New insights into aerosol and climate in the Arctic, *Atmos. Chem. Phys.*, 19, 2527–2560, <https://doi.org/10.5194/acp-19-2527-2019>, 2019.

480 Ahn, C., Yum, S. S., Park, M., Seo, P., Yoo, H-J., Lee, M., Lee, H.: Characteristics of new particle formation events occurred over the Yellow Sea in Springtime from 2019 to 2022, *Atmos. Res.*, 308, 107510, <https://doi.org/10.1016/j.atmosres.2024.107510>, 2024.

- 485 Health. Arctic Monitoring and Assessment Programme (AMAP), Tromsø, Norway. x + 375pp
- Angot, H., Blomquist, B., Howard, D., Archer, S., Bariteau, L., Beck, I., Boyer, M., Crotwell, M., Helmig, D., Hueber, J.,  
Jacobi, H.-W., Jokinen, T., Kulmala, M., Lan, X., Laurila, T., Madronich, M., Neff, D., Petäjä, T., Posman, K., Quéléver, L.,  
Shupe, M. D., Vimont, I., Schmale, J.: Year-round trace gas measurements in the central Arctic during the MOSAiC  
expedition. *Scientific Data*, 9(1), 723, <https://doi.org/10.1038/s41597-022-01769-6>, 2022.
- 490 Atmospheric Chemistry and Physics (ACP) POLARCAT (Polar Study using Aircraft, Remote Sensing, Surface Measurements  
and Models, of Climate, Chemistry, Aerosols, and Transport) special issue (last access: 29 Apr 2025), 2015.
- Barten, J. G.M., Ganzeveld, L. N., Steeneveld, G.-J., Blomquist, B. W., Angot, H., Archer, S. D., Bariteau, L., Beck, I., Boyer,  
M., von der Gathen, P., Helmig, D., Howard, D., Hueber, J., Jacobi, H.-W., Jokinen, T., Laurila, T., Posman, K. M., Quéléver,  
L., Schmale, J., Shupe, M. D., Krol, M. C.: Low ozone dry deposition rates to sea ice during the MOSAiC field campaign:  
495 Implications for the Arctic boundary layer ozone budget, *Elementa: Science of the Anthropocene*, 11 (1), 00086, doi:  
<https://doi.org/10.1525/elementa.2022.00086>, 2023.
- Bourgeois, I., Peischl, J., Thompson, C. R., Aikin, K. C., Campos, T., Clark, H., Commane, R., Daube, B., Diskin, G. W.,  
Elkins, J. W., Gao, R.-S., Gaudel, A., Hintsa, E. J., Johnson, B. J., Kivi, R., McKain, K., Moore, F. L., Parrish, D. D., Querel,  
R., Ray, E., Sánchez, R., Sweeney, C., Tarasick, D. W., Thompson, A. M., Thouret, V., Witte, J. C., Wofsy, S. C., and  
500 Ryerson, T. B.: Global-scale distribution of ozone in the remote troposphere from the ATom and HIPPO airborne field  
missions, *Atmos. Chem. Phys.*, 20, 10611–10635, <https://doi.org/10.5194/acp-20-10611-2020>, 2020.
- Boylan, P., Helmig, D., Oltmans, S.: Ozone in the Atlantic Ocean marine boundary layer, *Elementa: Science of the  
Anthropocene*, 3, 000045, <https://doi.org/10.12952/journal.elementa.000045>, 2015.
- Chambers, S.D., Williams, A.G., Crawford, J., Griffiths, A.D., Krummel, P.B., Steele, L.P., Law, R.M., van der Schoot, M.V.,  
505 Galbally, I.E., Molloy, S.B.: A radon-only technique for characterising “baseline” constituent concentrations at Cape Grim.  
In: Derek, N., Krummel, P.B., Cleland, S.J. (Eds.), *Baseline Atmospheric Program Australia 2011-2013*. Australian Bureau  
of Meteorology and CSIRO Marine and Atmospheric Research, 2018.
- Chang, K.-L., Cooper, O. R., Gaudel, A., Petropavlovskikh, I., Effertz, P., Morris, G., and McDonald, B. C.: Technical note:  
Challenges in detecting free tropospheric ozone trends in a sparsely sampled environment, *Atmos. Chem. Phys.*, 24, 6197–  
510 6218, <https://doi.org/10.5194/acp-24-6197-2024>, 2024.
- Chi, R., Obersteiner, F., Franchin, A., Campos, T., Bailey, A., Webster, C., Zahn, A., and Volkamer, R.: Intercomparison of  
fast airborne ozone instruments to measure eddy covariance fluxes: spatial variability in deposition at the ocean surface and  
evidence for cloud processing, *Atmos. Meas. Tech.*, 17, 5731–5746, <https://doi.org/10.5194/amt-17-5731-2024>, 2024.
- Coburn, S., Ortega, I., Thalman, R., Blomquist, B., Fairall, C. W., and Volkamer, R.: Measurements of diurnal variations and  
515 eddy covariance (EC) fluxes of glyoxal in the tropical marine boundary layer: description of the Fast LED-CE-DOAS  
instrument, *Atmos. Meas. Tech.*, 7, 3579–3595, <https://doi.org/10.5194/amt-7-3579-2014>, 2014.

Dickerson, R. R., Rhoads, K. P., Carsey, T. P., Oltmans, S. J., Burrows, J. P., and Crutzen, P. J.: Ozone in the remote marine boundary layer: A possible role for halogens, *J. Geophys. Res.*, 104(D17), 21385–21395, <https://doi.org/10.1029/1999JD900023>, 1999.

520 Draxler, R. R. and Rolph, G. D.: HYSPLIT (HYbrid Single-Particle Lagrangian Integrated Trajectory), NOAA Air Resources Laboratory, College Park, MD, USA, available at: <https://www.arl.noaa.gov/hysplit/hysplit/> (last access: 24 Nov 2024), 2013.

EBAS, <https://ebas-data.nilu.no/> (last access: 29 Apr 2025), 2025.

Fishman, J., Hoell Jr., J. M., Bendura, R. D., McNeal, R. J., Kirchhoff, V. W. J. H.: NASA GTE TRACE A experiment 525 (September–October 1992): Overview, *J. Geophys. Res.*, 101(D19), 23865–23879, <https://doi.org/10.1029/96JD00123>, 1996.

Forster, P., Storelvmo, T., Armour, K., Collins, W., Dufresne, J.-L., Frame, D., Lunt, D. J., Mauritsen, T., Palmer, M. D., 530 Watanabe, M., Wild, M., and Zhang, H.: The Earth’s Energy Budget, Climate Feedbacks, and Climate Sensitivity. In *Climate Change 2021: The Physical Science Basis. Contribution of Working Group I to the Sixth Assessment Report of the Intergovernmental Panel on Climate Change* [Masson-Delmotte, V., P. Zhai, A. Pirani, S.L. Connors, C. Péan, S. Berger, N. Caud, Y. Chen, L. Goldfarb, M.I. Gomis, M. Huang, K. Leitzell, E. Lonnoy, J.B.R. Matthews, T.K. Maycock, T. Waterfield, O. Yelekçi, R. Yu, and B. Zhou (eds.)]. Cambridge University Press, Cambridge, United Kingdom and New York, NY, USA, pp. 923–1054, <https://doi.org/10.1017/9781009157896.009>, 2021.

Fujiwara, M., Xie, S.-P., Shiotani, M., Hashizume, H., Hasebe, F., Vömel, H., Oltmans, S. J., Watanabe, T.: Upper-535 tropospheric inversion and easterly jet in the tropics, *J. Geophys. Res.*, 108 (D24), 2796, <https://doi.org/10.1029/2003JD003928>, 2003.

Galbally, I. E., Bentley, S. T., and Meyer, C. P.: Mid-latitude marine boundary layer ozone destruction at visible sunrise observed at Cape Grim, Tasmania, 41° S, *Geophys. Res. Lett.*, 27, 3841–3844, <https://doi.org/10.1029/1999GL010943>, 2000.

Ganzeveld, L., Helmig, D., Fairall, C., Hare, J., and Pozzer, A.: Atmosphere-ocean ozone exchange: A global modeling study 540 of biogeochemical, atmospheric, and waterside turbulence dependencies, *Global Biogeochem. Cy.*, 23, 4, <https://doi.org/10.1029/2008GB003301>, 2009.

Gaudel, A., Bourgeois, I., Li, M., Chang, K.-L., Ziemke, J., Sauvage, B., Stauffer, R. M., Thompson, A. M., Kollonige, D. E., Smith, N., Hubert, D., Keppens, A., Cuesta, J., Heue, K.-P., Veefkind, P., Aikin, K., Peischl, J., Thompson, C. R., Ryerson, T. B., Frost, G. J., McDonald, B. C., and Cooper, O. R.: Tropical tropospheric ozone distribution and trends from in situ and 545 satellite data, *Atmos. Chem. Phys.*, 24, 9975–10000, <https://doi.org/10.5194/acp-24-9975-2024>, 2024.

Gómez Martín, J. C., H. Vömel, T. D. Hay, A. S. Mahajan, C. Ordóñez, M. C. Parrondo Sempere, M. Gil-Ojeda, and A. Saiz-Lopez, On the variability of ozone in the equatorial eastern Pacific boundary layer, *J. Geophys. Res. Atmos.*, 121, 11,086–11,103, <https://doi.org/10.1002/2016JD025392>, 2016.

Gong, W., Beagley, S. R., Toyota, K., Skov, H., Christensen, J. H., Lupu, A., Pendlebury, D., Zhang, J., Im, U., Kanaya, Y., 550 Saiz-Lopez, A., Sommariva, R., Effertz, P., Halfacre, J. W., Jepsen, N., Kivi, R., Koenig, T. K., Müller, K., Nordstrøm, C.,

Petropavlovskikh, I., Shepson, P. B., Simpson, W. R., Solberg, S., Staebler, R. M., Tarasick, D. W., Van Malderen, R., and Vestenius, M.: Modelling Arctic Lower Tropospheric Ozone: processes controlling seasonal variations, EGUsphere [preprint], <https://doi.org/10.5194/egusphere-2024-3750>, 2025.

Griffiths, P. T., Murray, L. T., Zeng, G., Shin, Y. M., Abraham, N. L., Archibald, A. T., Deushi, M., Emmons, L. K., Galbally, 555 I. E., Hassler, B., Horowitz, L. W., Keeble, J., Liu, J., Moeini, O., Naik, V., O'Connor, F. M., Oshima, N., Tarasick, D., Tilmes, S., Turnock, S. T., Wild, O., Young, P. J., and Zanis, P.: Tropospheric ozone in CMIP6 simulations, *Atmos. Chem. Phys.*, 21, 4187–4218, <https://doi.org/10.5194/acp-21-4187-2021>, 2021.

Halfacre, J. W., Knepp, T. N., Shepson, P. B., Thompson, C. R., Pratt, K. A., Li, B., Peterson, P. K., Walsh, S. J., Simpson, 560 W. R., Matrai, P. A., Bottenheim, J. W., Netcheva, S., Perovich, D. K., and Richter, A.: Temporal and spatial characteristics of ozone depletion events from measurements in the Arctic, *Atmos. Chem. Phys.*, 14, 4875–4894, <https://doi.org/10.5194/acp-14-4875-2014>, 2014.

Hardacre, C., Wild, O., and Emberson, L.: An evaluation of ozone dry deposition in global scale chemistry climate models, *Atmos. Chem. Phys.*, 15, 6419–6436, <https://doi.org/10.5194/acp-15-6419-2015>, 2015.

Harris, J. M. and Oltmans, S. J.: Variations in tropospheric ozone related to transport at American Samoa, *J. Geophys. Res.*, 565 102 (D7), 8781–8791, 1997.

[Harris, J. M., Draxler, R. R., Oltmans, S. J.: Trajectory model sensitivity to differences in input data and vertical transport method, J. Geophys. Res., 110, D14109, http://doi:10.1029/2004JD005750, 2005.](#)

Harriss, R. C., Garstang, M., Wofsy, S. C., Beck, S. M., Bendura, R. J., Coelho, J. R. B., Drewry, J. W., Hoell Jr., J. M., Matson, P. A., McNeal, R. J., Molion, L. C. B., Navarro, R. L., Rabine, V., Snell, R. L.: The Amazon Boundary Layer 570 Experiment: Wet season 1987, *J. Geophys. Res.*, 95(D10), 16721–16736, <https://doi.org/10.1029/JD095iD10p16721>, 1990.

Harriss, R. C., Wofsy, S. C., Hoell Jr., J. M., Bendura, R. J., Drewry, J. W., McNeal, R. J., Pierce, D., Rabine, V., Snell, R. L.: The Arctic Boundary Layer Expedition (ABLE-3B): July–August 1990, *J. Geophys. Res.*, 99(D1), 1635–1643, <https://doi.org/10.1029/93JD01788>, 1994.

Harriss, R. C., Wofsy, S. C., Bartlett, D. S., Shipham, M. C., Jacob, D. J., Hoell Jr., J. M., Bendura, R. J., Drewry, J. W., 575 McNeal, R. J., Navarro, R. L., Gidge, R. N., Rabine, V. E.: The Arctic Boundary Layer Expedition (ABLE 3A): July–August 1988, *J. Geophys. Res.*, 97(D15), 16383–16394, <https://doi.org/10.1029/91JD02109>, 1992.

Helmig, D., Lang, E. K., Bariteau, L., Boylan, P., Fairall, C. W., Ganzeveld, L., Hare, J. E., Hueber, J., and Pallandt, M.: Atmosphere-ocean ozone fluxes during the TexAQS 2006, STRATUS 2006, GOMECC 2007, GasEx 2008, and AMMA 2008 cruises, *J. Geophys. Res.-Atmos.*, 117, D4, <https://doi.org/10.1029/2011JD015955>, 2012.

Hoell Jr., J. M., Davis, D. D., Gregory, G. L., McNeal, R. J., Bendura, R. J., Drewry, J. W., Barrick, J. D., Kirchhoff, V. W. J. H., Motta, A. G., Navarro, R. L., Dorko, W. D., Owen, D. W.: Operational overview of the NASA GTE/CITE 3 airborne instrument intercomparisons for sulfur dioxide, hydrogen sulfide, carbonyl sulfide, dimethyl sulfide, and carbon disulfide, *J. Geophys. Res.*, 98(D12), 23291–23304, <https://doi.org/10.1029/93JD00453>, 1993.

- Hoell, J. M., Davis, D. D., Jacob, D. J., Rodgers, M. O., Newell, R. E., Fuelberg, H. E., McNeal, R. J., Raper, J. L., Bendura, R. J.: Pacific Exploratory Mission in the tropical Pacific: PEM-Tropics A, August-September 1996, *J. Geophys. Res.*, 104(D5), 5567–5583, 1999.
- Hoell, J. M., Davis, D. D., Liu, S. C., Newell, R. E., Akimoto, H., McNeal, R. J., Bendura, R. J.: The Pacific Exploratory Mission-West Phase B: February-March, 1994, *J. Geophys. Res.*, 102(D23), 28223–28239, <https://doi.org/10.1029/97JD02581>, 1997.
- Hoell, J. M., Davis, D. D., Liu, S. C., Newell, R., Shipham, M., Akimoto, H., McNeal, R. J., Bendura, R. J., J. W. Drewry: Pacific Exploratory Mission-West A (PEM-West A): September–October 1991, *J. Geophys. Res.*, 101(D1), 1641–1653, <https://doi.org/10.1029/95JD00622>, 1996.
- Hu, X.-M., Sigler, J. M., Fuentes, J. D.: Variability of ozone in the marine boundary layer of the equatorial Pacific Ocean, *J. Atmos. Chem.*, 66, 117–136, 2010.
- Inamdar, S., Tinel, L., Chance, R., Carpenter, L. J., Sabu, P., Chacko, R., Tripathy, S. C., Kerkar, A. U., Sinha, A. K., Bhaskar, P. V., Sarkar, A., Roy, R., Sherwen, T. T., Cuevas, C., Saiz-Lopez, A., Ram, K., Mahajan, A. S.: Estimation of Reactive Inorganic Iodine Fluxes in the Indian and Southern Ocean Marine Boundary Layer, *Atmos. Chem. Phys.*, 20, 12093–12114, <https://doi.org/10.5194/acp-20-12093-2020>, 2020.
- Jacob, D. J., Crawford, J. H., Maring, H., Clarke, A. D., Dibb, J. E., Emmons, L. K., Ferrare, R. A., Hostetler, C. A., Russell, P. B., Singh, H. B., Thompson, A. M., Shaw, G. E., McCauley, E., Pederson, J. R., and Fisher, J. A.: The Arctic Research of the Composition of the Troposphere from Aircraft and Satellites (ARCTAS) mission: design, execution, and first results, *Atmos. Chem. Phys.*, 10, 5191–5212, <https://doi.org/10.5194/acp-10-5191-2010>, 2010.
- Jacob, D. J., Crawford, J. H., Kleb, M. M., Connors, V. S., Bendura, R. J., Raper, J. L., Sachse, G. W., Gille, J. C., Emmons, L., Heald, C. L.: Transport and Chemical Evolution over the Pacific (TRACE-P) aircraft mission: Design, execution, and first results, *J. Geophys. Res.*, 108 (D20), 9000, <https://doi.org/10.1029/2002JD003276>, 2003.
- Johnson, J. E., Gammon, R. H., Larsen, J., Bates, T. S., Oltmans, S. J., and Farmer, J. C.: Ozone in the marine boundary layer over the Pacific and Indian Oceans: Latitudinal gradients and diurnal cycles, *J. Geophys. Res.*, 95(D8), 11847–11856, <https://doi.org/10.1029/JD095iD08p11847>, 1990.
- Kanaya, Y., Miyazaki, K., Taketani, F., Miyakawa, T., Takashima, H., Komazaki, Y., Pan, X., Kato, S., Sudo, K., Sekiya, T., Inoue, J., Sato, K., and Oshima, K.: Ozone and carbon monoxide observations over open oceans on R/V *Mirai* from 67° S to 75° N during 2012 to 2017: testing global chemical reanalysis in terms of Arctic processes, low ozone levels at low latitudes, and pollution transport, *Atmos. Chem. Phys.*, 19, 7233–7254, <https://doi.org/10.5194/acp-19-7233-2019>, 2019.
- Kanaya, Y. et al., Observational ozone data over the global oceans and polar regions: The TOAR-II Oceans data-set version 2025, <https://doi.org/10.17596/0004044>, 2025.
- Kleb, M. M., Chen, G., Crawford, J. H., Flocke, F. M., and Brown, C. C.: An overview of measurement comparisons from the INTEX-B/MILAGRO airborne field campaign, *Atmos. Meas. Tech.*, 4, 9–27, <https://doi.org/10.5194/amt-4-9-2011>, 2011.

- Law, K. S., Hjorth, J. L., Pernov, J. B., Whaley, C. H., Skov, H., Collaud Coen, M., Langner, J., Arnold, S. R., Tarasick, D., Christensen, J., Deushi, M., Effertz, P., Faluvegi, G., Gauss, M., Im, U., Oshima, N., Petropavlovskikh, I., Plummer, D., Tsigaridis, K., Tsyro, S., Solberg, S., Turnock, S. T.: Arctic tropospheric ozone trends, *Geophys. Res. Lett.*, 50, e2023GL103096, <https://doi.org/10.1029/2023GL103096>, 2023.
- 620 Lelieveld, J., Van Aardenne, J., Fischer, H., De Reus, M., Williams, J., and Winkler, P.: Increasing ozone over the Atlantic Ocean, *Science*, 304, 1483–1487, 2004.
- Luhar, A. K., Woodhouse, M. T., and Galbally, I. E.: A revised global ozone dry deposition estimate based on a new two-layer parameterisation for air–sea exchange and the multi-year MACC composition reanalysis, *Atmos. Chem. Phys.*, 18, 4329–4348, <https://doi.org/10.5194/acp-18-4329-2018>, 2018.
- 625 Mahajan, A. S., Tiné, L., Sarkar, A., Chance, R., Carpenter, L. J., Hulswar, S., Mali, P., Prakash, S., & Vinayachandran, P. N.: Understanding Iodine Chemistry over the Northern and Equatorial Indian Ocean. *J. Geophys. Res. Atmos.*, 124, 8104–8118, <https://doi.org/10.1029/2018JD029063>, 2019.
- Monks, P.S., Carpenter, L.J., Penkett, S.A., Ayers, G.P., Gillett, R.W., Galbally, I.E., Meyer, C.P., Fundamental ozone photochemistry in the remote marine boundary layer: the SOAPEX experiment, measurement and theory, *Atmos. Environ.*, 32, 3647–3664, 1998.
- 630 Nagao, I., Matsumoto, K., Tanaka, H.: Sunrise ozone destruction found in the sub-tropical marine boundary layer, *Geophys. Res. Lett.*, 26 3377–3380, 1999.
- NASA, [https://lads.gsfc.nasa.gov/gldas/data/0.25deg/landmask\\_mod44w\\_025.asc](https://lads.gsfc.nasa.gov/gldas/data/0.25deg/landmask_mod44w_025.asc) (last access: 27 May 2019), 2019.
- 635 Oltmans, S. J.: Surface ozone measurements in clean air, *J. Geophys. Res.*, 86(C2), 1174–1180, <https://doi.org/10.1029/JC086iC02p01174>, 1981.
- Pan, L., Atlas, E., Salawitch, R., Honomichl, S., Bresch, J., Randel, W., Apel, E., Hornbrook, R., Weinheimer, A., Anderson, D., Andrews, S., Baidar, S., Beaton, S., Campos, T., Carpenter, L., Chen, D., Dix, B., Donets, V., Hall, S., Hanisco, T., Homeyer, C., Huey, L., Jensen, J., Kaser, L., Kinnison, D., Koenig, T., Lamarque, J., Liu, C., Luo, J., Luo, Z., Montzka, D., Nicely, J., Pierce, R., Riemer, D., Robinson, T., Romashkin, P., Saiz-Lopez, A., Schauffler, S., Shieh, O., Stell, M., Ullmann, K., Vaughan, G., Volkamer, R. and Wolfe, G.: The Convective Transport of Active Species in the Tropics (CONTRAST) Experiment, *Bull. Amer. Meteorol. Soc.*, 98(1), 106–128, <https://doi.org/10.1175/BAMS-D-14-00272.1>, 2017.
- 640 Parrish, D. D., Millet, D. B., and Goldstein, A. H.: Increasing ozone in marine boundary layer inflow at the west coasts of North America and Europe, *Atmos. Chem. Phys.*, 9, 1303–1323, <https://doi.org/10.5194/acp-9-1303-2009>, 2009.
- Pollack, I. B., Lerner, B. T., and Ryerson, T. B.: Evaluation of ultraviolet light-emitting diodes for detection of atmospheric NO<sub>2</sub> by photolysis-chemiluminescence, *J. Atmos. Chem.*, 65, 111–125, <https://doi.org/10.1007/s10874-011-9184-3>, 2011.
- Pope, R. J., Kerridge, B. J., Siddans, R., Latter, B. G., Chipperfield, M. P., Feng, W., Pimlott, M. A., Dhomse, S. S., Retscher, C., and Rigby, R.: Investigation of spatial and temporal variability in lower tropospheric ozone from RAL Space UV–Vis satellite products, *Atmos. Chem. Phys.*, 23, 14933–14947, <https://doi.org/10.5194/acp-23-14933-2023>, 2023.

- 650 Pound, R. J., Sherwen, T., Helmg, D., Carpenter, L. J., and Evans, M. J.: Influences of oceanic ozone deposition on tropospheric photochemistry, *Atmos. Chem. Phys.*, 20, 4227–4239, <https://doi.org/10.5194/acp-20-4227-2020>, 2020.
- Prados-Roman, C., Cuevas, C. A., Hay, T., Fernandez, R. P., Mahajan, A. S., Royer, S.-J., Galí, M., Simó, R., Dachs, J., Großmann, K., Kinnison, D. E., Lamarque, J.-F., and Saiz-Lopez, A.: Iodine oxide in the global marine boundary layer, *Atmos. Chem. Phys.*, 15, 583–593, <https://doi.org/10.5194/acp-15-583-2015>, 2015.
- 655 Raper, J. L., Kleb, M. M., Jacob, D. J., Davis, D. D., Newell, R. E., Fuelberg, H. E., Bendura, R. J., Hoell, J. M., McNeal, R. J.: Pacific Exploratory Mission in the Tropical Pacific: PEM-Tropics B, March-April 1999, *J. Geophys. Res.*, 106(D23), 32401–32425, <https://doi.org/10.1029/2000JD900833>, 2001.
- Read, K. A., Mahajan, A. S., Carpenter, L. J., Evans, M. J., Faria, B. V. E., Heard, D. E., Hopkins, J. R., Lee, J. D., Moller, S. J., Lewis, A. C., Mendes, L., McQuaid, J. B., Oetjen, H., Saiz-Lopez, A., Pilling, M. J., and Plane, J. M. C.: Extensive halogen mediated ozone destruction over the tropical Atlantic Ocean, *Nature*, 453, 1232–1235, 2008.
- 660 Ryerson, T. B., Buhr, M. P., Frost, G. J., Goldan, P. D., Holloway, J. S., Hübner, G., Jobson, B. T., Kuster, W. C., McKeen, S. A., Parrish, D. D., Roberts, J. M., Sueper, D. T., Trainer, M., Williams, J., Fehsenfeld, F. C.: Emissions lifetimes and ozone formation in power plant plumes, *J. Geophys. Res.*, 103(D17), 22569–22583, <https://doi.org/10.1029/98JD01620>, 1998.
- Saiz-Lopez, A. von Glasow, R.: Reactive halogen chemistry in the troposphere. *Chem. Soc. Rev.*, 41, 6448–6472, 2012.
- 665 Sarwar, G., Kang, D., Foley, K., Schwede, D., and Gantt, B.: Technical note: Examining ozone deposition over seawater, *Atmos. Environ.*, 141, 255–262, <https://doi.org/10.1016/j.atmosenv.2016.06.072>, 2016.
- Schultz, M. G., Schröder, S., Lyapina, O., Cooper, O. R., Galbally, I., Petropavlovskikh, I., von Schneidemesser, E., Tanimoto, H., Elshorbany, Y., Naja, M., Seguel, R. J., Dauert, U., Eckhardt, P., Feigenspan, S., Fiebig, M., Hjellbrekke, A.-G., Hong, Y.-D., Kjeld, P. C., Koide, H., Lear, G., Tarasick, D., Ueno, M., Wallasch, M., Baumgardner, D., Chuang, M.-T., Gillett, R., Lee, M., Molloy, S., Moolla, R., Wang, T., Sharps, K., Adame, J. A., Ancellet, G., Apadula, F., Artaxo, P., Barlasina, M. E., Bogucka, M., Bonasoni, P., Chang, L., Colomb, A., Cuevas, Agulló, E., Cupeiro, M., Degorska, A., Ding, A., Fröhlich, M., Frolova, M., Gadhavi, H., Gheusi, F., Gilge, S., Gonzalez, M. Y., Gros, V., Hamad, S. H., Helmg, D., Henriques, D., Hermansen, O., Holla, R., Hueber, J., Im, U., Jaffe, D. A., Komala, N., Kubistin, D., Lam, K. -S., Laurila, T., Lee, H., Levy, I., Mazzoleni, C., Mazzoleni, L. R., McClure-Begley, A., Mohamad, M., Murovec, M., Navarro-Comas, M., Nicodim, F., Parrish, D., Read, K. A., Reid, N., Ries, L., Saxena, P., Schwab, J. J., Scorgie, Y., Senik, I., Simmonds, P., Sinha, V., Skorokhod, A. I., Spain, G., Spangl, W., Spoor, R., Springston, S. R., Steer, K., Steinbacher, M., Suharguniyanwan, E., Torre, P., Trickl, T., Weili, L., Weller, R., Xiaobin, X., Xue, L., and Zhiqiang, M.: Tropospheric Ozone Assessment Report: Database and metrics data of global surface ozone observations, *Elementa: Science of the Anthropocene*, 5,1582, <https://doi.org/10.1525/elementa.244>, 2017.
- 675 Sekiya, T., Kanaya, Y., Sudo, K., Taketani, F., Iwamoto, Y., Aita, M. N., Yamamoto, A., and Kawamoto, K.: Global Bromine- and Iodine-Mediated Tropospheric Ozone Loss Estimated Using the CHASER Chemical Transport Model, *Sola*, 16, 220–227, <https://doi.org/10.2151/sola.2020-037>, 2020.

- Shiotani, M., Fujiwara, M., Hasebe, F., Hashizume, H., Vömel, H., Oltmans, S. J., Watanabe, T.: Ozonesonde observations in the equatorial Eastern Pacific - the Shoyo-maru survey -, *J. Meteorol. Soc. Jpn.*, 80, No. 4B, 897-909,  
685 <https://doi.org/10.2151/jmsj.80.897>, 2002.
- Shon, Z.-H., Madronich, S., Song, S.-K., Flocke, F. M., Knapp, D. J., Anderson, R. S., Shetter, R. E., Cantrell, C. A., Hall, S.  
R., and Tie, X.: Characteristics of the NO-NO<sub>2</sub>-O<sub>3</sub> system in different chemical regimes during the MIRAGE-Mex field  
campaign, *Atmos. Chem. Phys.*, 8, 7153–7164, <https://doi.org/10.5194/acp-8-7153-2008>, 2008.
- Schröder, S., Schultz, M. G., Selke, N., Sun, J., Ahring, J., Mozaffari, A., Romberg, M., Epp, E., Lensing, M., Apweiler, S.,  
690 Leufen, L. H., Betancourt, C., Hagemeier, B., Rajveer, S.: TOAR Data Infrastructure; <https://doi.org/10.34730/4d9a287dec0b42f1aa6d244de8f19eb3>; <https://toar-data.org/surface-data/> (last access: 29 Apr  
2025), 2024.
- Simpson, W. R., von Glasow, R., Riedel, K., Anderson, P., Ariya, P., Bottenheim, J., Burrows, J., Carpenter, L. J., Frieß, U.,  
Goodsite, M. E., Heard, D., Hutterli, M., Jacobi, H.-W., Kaleschke, L., Neff, B., Plane, J., Platt, U., Richter, A., Roscoe, H.,  
695 Sander, R., Shepson, P., Sodeau, J., Steffen, A., Wagner, T., and Wolff, E.: Halogens and their role in polar boundary-layer  
ozone depletion, *Atmos. Chem. Phys.*, 7, 4375–4418, <https://doi.org/10.5194/acp-7-4375-2007>, 2007.
- Simpson, W. R., Brown, S. S., Saiz-Lopez, A., Thornton, J. A. and Von Glasow, R.: Tropospheric halogen chemistry: sources,  
cycling, and impacts, *Chem. Rev.*, 115, 4035–4062, 2015.
- Singh, H. B., Brune, W. H., Crawford, J. H., Flocke, F., and Jacob, D. J.: Chemistry and transport of pollution over the Gulf  
700 of Mexico and the Pacific: spring 2006 INTEX-B campaign overview and first results, *Atmos. Chem. Phys.*, 9, 2301–2318,  
<https://doi.org/10.5194/acp-9-2301-2009>, 2009.
- Singh, H. B., Brune, W. H., Crawford, J. H., Jacob, D. J., and Russell, P. B.: Overview of the summer 2004 Intercontinental  
Chemical Transport Experiment–North America (INTEX-A), *J. Geophys. Res.*, 111, D24S01,  
<http://doi.org/10.1029/2006JD007905>, 2006.
- 705 Stone, D., Sherwen, T., Evans, M. J., Vaughan, S., Ingham, T., Whalley, L. K., Edwards, P. M., Read, K. A., Lee, J. D., Moller,  
S. J., Carpenter, L. J., Lewis, A. C., and Heard, D. E.: Impacts of bromine and iodine chemistry on tropospheric OH and  
HO<sub>2</sub>: comparing observations with box and global model perspectives, *Atmos. Chem. Phys.*, 18, 3541–3561,  
<https://doi.org/10.5194/acp-18-3541-2018>, 2018.
- Szopa, S., Naik, V., Adhikary, B., Artaxo, P., Berntsen, T., Collins, W. D., Fuzzi, S., Gallardo, L., Kiendler-Scharr, A., Klimont,  
710 Z., Liao, H., Unger, N., and Zanis, P.: Short-Lived Climate Forcers. In *Climate Change 2021: The Physical Science Basis. Contribution of Working Group I to the Sixth Assessment Report of the Intergovernmental Panel on Climate Change* [Masson-Delmotte, V., P. Zhai, A. Pirani, S.L. Connors, C. Péan, S. Berger, N. Caud, Y. Chen, L. Goldfarb, M.I. Gomis, M. Huang, K. Leitzell, E. Lonnoy, J.B.R. Matthews, T.K. Maycock, T. Waterfield, O. Yelekçi, R. Yu, and B. Zhou (eds.)]. Cambridge University Press, Cambridge, United Kingdom and New York, NY, USA, pp. 817–922, <https://doi.org/10.1017/9781009157896.008>, 2021.

Thompson, A. M., Johnson, J. E., Torres, A. L., Bates, T. S., Kelly, L. C., Atlas, E., Greenberg, J. P., Donahue, N. M., Yvon, S. A., Saltzman, E. S., Heikes, B. G., Mosher, B. W., Shashkov, A. A., Yegorov, V. I.: Ozone observations and a model of marine boundary layer photochemistry during SAGA 3, *J. Geophys. Res.*, 98(D9), 16955–16968, <https://doi.org/10.1029/93JD00258>, 1993.

720 TOAR-II Steering Committee, TOAR-II Community Special Issue Guidelines: [https://igacproject.org/sites/default/files/2023-04/TOAR-II\\_Community\\_Special\\_Issue\\_Guidelines\\_202304.pdf](https://igacproject.org/sites/default/files/2023-04/TOAR-II_Community_Special_Issue_Guidelines_202304.pdf) (last access: 29 Apr 2025), 2023.

Tulet, P., Van Baelen, J., Bosscher, P., Brioude, J., Colomb, A., Goloub, P., Pazmino, A., Portafaix, T., Ramonet, M., Sellegri, K., Thyssen, M., Gest, L., Marquestaut, N., Mékiès, D., Metzger, J.-M., Athier, G., Blarel, L., Delmotte, M., Desprairies, G., Dournaux, M., Dubois, G., Duflot, V., Lamy, K., Gardes, L., Guillemot, J.-F., Gros, V., Kolasinski, J., Lopez, M.,  
725 Magand, O., Noury, E., Nunes-Pinharanda, M., Payen, G., Pianezze, J., Picard, D., Picard, O., Prunier, S., Rigaud-Louise, F., Sicard, M., and Torres, B.: MAP-IO: an atmospheric and marine observatory program on board Marion Dufresne over the Southern Ocean, *Earth Syst. Sci. Data*, 16, 3821–3849, <https://doi.org/10.5194/essd-16-3821-2024>, 2024.

Ueda, S., Iwamoto, Y., Taketani, F., Liu, M., and Matsui, H.: Morphological features and water solubility of iron in aged fine aerosol particles over the Indian Ocean, *Atmos. Chem. Phys.*, 23, 10117–10135, <https://doi.org/10.5194/acp-23-10117-2023>,  
730 2023.

Van Malderen, R., Thompson, A. M., Kollonige, D. E., Stauffer, R. M., Smit, H. G. J., Maillard Barras, E., Vigouroux, C., Petropavlovskikh, I., Leblanc, T., Thouret, V., Wolff, P., Effertz, P., Tarasick, D. W., Poyraz, D., Ancellet, G., De Backer, M.-R., Evan, S., Flood, V., Frey, M. M., Hannigan, J. W., Hernandez, J. L., Iarlori, M., Johnson, B. J., Jones, N., Kivi, R., Mahieu, E., McConville, G., Müller, K., Nagahama, T., Notholt, J., Piters, A., Prats, N., Querel, R., Smale, D., Steinbrecht, W., Strong, K., and Sussmann, R.: Global Ground-based Tropospheric Ozone Measurements: Reference Data and Individual Site Trends (2000–2022) from the TOAR-II/HEGIFTOM Project, EGUSphere [preprint], <https://doi.org/10.5194/egusphere-2024-3736>, 2025.

Volkamer, R., Baidar, S., Campos, T. L., Coburn, S., DiGangi, J. P., Dix, B., Eloranta, E. W., Koenig, T. K., Morley, B., Ortega, I., Pierce, B. R., Reeves, M., Sinreich, R., Wang, S., Zondlo, M. A., and Romashkin, P. A.: Aircraft measurements of BrO, IO, glyoxal, NO<sub>2</sub>, H<sub>2</sub>O, O<sub>2</sub>–O<sub>2</sub> and aerosol extinction profiles in the tropics: comparison with aircraft-/ship-based in situ and lidar measurements, *Atmos. Meas. Tech.*, 8, 2121–2148, <https://doi.org/10.5194/amt-8-2121-2015>, 2015.

Watanabe, K., Nojiri, Y., Kariya, S.: Measurements of ozone concentrations on a commercial vessel in the marine boundary layer over the northern North Pacific Ocean, *J. Geophys. Res.*, 110, D11310, [http://doi.org/10.1029/2004JD005514](https://doi.org/10.1029/2004JD005514), 2005.

Whaley, C. H., Law, K. S., Hjorth, J. L., Skov, H., Arnold, S. R., Langner, J., Pernov, J. B., Bergeron, G., Bourgeois, I.,  
745 Christensen, J. H., Chien, R.-Y., Deushi, M., Dong, X., Effertz, P., Faluvegi, G., Flanner, M., Fu, J. S., Gauss, M., Huey, G., Im, U., Kivi, R., Marelle, L., Onishi, T., Oshima, N., Petropavlovskikh, I., Peischl, J., Plummer, D. A., Pozzoli, L., Raut, J.-C., Ryerson, T., Skeie, R., Solberg, S., Thomas, M. A., Thompson, C., Tsagaridis, K., Tsyro, S., Turnock, S. T., von Salzen, K., and Tarasick, D. W.: Arctic tropospheric ozone: assessment of current knowledge and model performance, *Atmos. Chem. Phys.*, 23, 637–661, <https://doi.org/10.5194/acp-23-637-2023>, 2023.

- 750 Whittlestone, S., Gras, J. L., and Siems, S. T.: Surface air mass origins during the First Aerosol Characterization Experiment (ACE 1), *J. Geophys. Res.*, 103(D13), 16341–16350, 1998.
- Wofsy, S. C., Daube, B. C., Jimenez, R., Kort, E., Pittman, J. V., Park, S., Commane, R., Xiang, B., Santoni, G., Jacob, D., Fisher, J., Pickett-Heaps, C., Wang, H., Wecht, K., Wang, Q.-Q., Stephens, B. B., Shertz, S., Watt, A.S., Romashkin, P., Campos, T., Haggerty, J., Cooper, W. A., Rogers, D., Beaton, S., Hendershot, R., Elkins, J. W., Fahey, D. W., Gao, R. S.,  
755 Moore, F., Montzka, S. A., Schwarz, J. P., Perring, A. E., Hurst, D., Miller, B. R., Sweeney, C., Oltmans, S., Nance, D., Hintsa, E., Dutton, G., Watts, L. A., Spackman, J. R., Rosenlof, K. H., Ray, E. A., Hall, B., Zondlo, M. A., Diao, M., Keeling, R., Bent, J., Atlas, E. L., Lueb, R., Mahoney, M. J.: HIPPO Merged 10-second Meteorology, Atmospheric Chemistry, and Aerosol Data. Version 1.0. UCAR/NCAR – Earth Observing Laboratory, [http://doi.org/10.3334/CDIAC/HIPPO\\_010](http://doi.org/10.3334/CDIAC/HIPPO_010) (CDIAC Release 20121129/ NCAR EOL Version 1.0), 2017.
- 760 Wofsy, S. C., Afshar, S., Allen, H. M., Apel, E. C., Asher, E. C., Barletta, B., Bent, J., Bian, H., Biggs, B. C., Blake, D. R., Blake, N., Bourgeois, I., Brock, C. A., Brune, W. H., Budney, J. W., Bui, T. P., Butler, A., Campuzano-Jost, P., Chang, C. S., Chin, M., Commane, R., Correa, G., Crounse, J. D., Cullis, P. D., Daube, B. C., Day, D. A., Dean-Day, J. M., Dibb, J. E., DiGangi, J. P., Diskin, G. S., Dollner, M., Elkins, J. W., Erdesz, F., Fiore, A. M., Flynn, C. M., Froyd, K. D., Gesler, D. W., Hall, S. R., Hanisco, T. F., Hannun, R. A., Hills, A. J., Hintsa, E. J., Hoffman, A., Hornbrook, R. S., Huey, L. G.,  
765 Hughes, S., Jimenez, J. L., Johnson, B. J., Katich, J. M., Keeling, R. F., Kim, M. J., Kupc, A., Lait, L. R., McKain, K., McLaughlin, R. J., Meinardi, S., Miller, D. O., Montzka, S. A., Moore, F. L., Morgan, E. J., Murphy, D. M., Murray, L. T., Nault, B. A., Neuman, J. A., Newman, P. A., Nicely, J. M., Pan, X., Paplawsky, W., Peischl, J., Prather, M. J., Price, D. J., Ray, E. A., Reeves, J. M., Richardson, M., Rollins, A. W., Rosenlof, K. H., Ryerson, T. B., Scheuer, E., Schill, G. P., Schroder, J. C., Schwarz, J. P., St.Clair, J. M., Steenrod, S. D., Stephens, B. B., Strode, S. A., Sweeney, C., Tanner, D., Teng, A. P., Thamess, A. B., Thompson, C. R., Ullmann, K., Veres, P. R., Wagner, N. L., Watt, A., Weber, R., Weinzierl, B. B., Wennberg, P. O., Williamson, C. J., Wilson, J. C., Wolfe, G. M., Woods, C. T., Zeng, L. H., and Vieznor, N.: ATom: Merged Atmospheric Chemistry, Trace Gases, and Aerosols, Version 2. ORNL DAAC, Oak Ridge, Tennessee, USA, <https://doi.org/10.3334/ORNLDaac/1925>, 2021.
- 770 Young, P. J., Naik, V., Fiore, A. M., Gaudel, A., Guo, J., Lin, M. Y., Neu, J. L., Parrish, D. D., Rieder, H. E., Schnell, J. L., Tilmes, S., Wild, O., Zhang, L., Ziemke, J. R., Brandt, J., Delcloo, A., Doherty, R. M., Geels, C., Hegglin, M. I., Hu, L., Im, U., Kumar, R., Luhar, A., Murray, L., Plummer, D., Rodriguez, J., Saiz-Lopez, A., Schultz, M.G., Woodhouse, M. T. and Zeng, G.: Tropospheric Ozone Assessment Report: Assessment of global-scale model performance for global and regional ozone distributions, variability, and trends, *Elem. Sci. Anth.*, 6, p. 10, <https://doi.org/10.1525/elementa.265>, 2018.
- Zhang, B., Liu, H., Crawford, J. H., Chen, G., Fairlie, T. D., Chambers, S., Kang, C.-H., Williams, A. G., Zhang, K., Considine, D. B., Sulprizio, M. P., and Yantosca, R. M.: Simulation of radon-222 with the GEOS-Chem global model: emissions, seasonality, and convective transport, *Atmos. Chem. Phys.*, 21, 1861–1887, <https://doi.org/10.5194/acp-21-1861-2021>, 2021.



**Table 1.** List of cruise/buoy data contained in the ship/buoy data file.

Label	Cruise	Platform	Reso_- lution	Year	Data number	Ancillary data	Instrument	Uncertainty	PI/ Data Manager/ WG member worked on the data]	Regions	Literature	Data source
S1	MR12: MR12- 02	Mirai	1 h	2012	733	CO	Thermo, 49C	1%	Yugo Kanaya	R1	Kanaya et al. (2019)	
S2	MR13: MR13- 01, 02	Mirai	1 h	2013	2605	CO	Thermo, 49C	1%	Yugo Kanaya	R1,2,4,10	Kanaya et al. (2019)	
S3	MR14: MR14- 04, 05, 06	Mirai	1 h	2014	3561	CO	Thermo, 49C	1%	Yugo Kanaya	R1,2,4,10	Kanaya et al. (2019)	
S4	MR15: MR15- 03, 04, 05	Mirai	1 h	2015	2374	CO	Thermo, 49C	1%	Yugo Kanaya	R1,2,5,10	Kanaya et al. (2019)	
S5	MR16: MR16- 06, 08, 09	Mirai	1 h	2016	2393	CO	Thermo, 49C	1%	Yugo Kanaya	R1,2,3,10,1	Kanaya et al. (2019)	
S6	MR17: MR17- 05C, 08	Mirai	1 h	2017	2662	CO	Thermo, 49C	1%	Yugo Kanaya	R1,2,4,10		DOI: 10.17596/0001879, 10.17596/0001881, 10.17596/0001882
S7	MR18: MR18- 04, 05C, 06	Mirai	1 h	2018	2567	CO	Thermo, 49C	1%	Yugo Kanaya	R1,2,3,10,1		DOI: 10.17596/0001886, 10.17596/0001887, 10.17596/0001888, 10.17596/0001889, 10.17596/0001976
S8	MR19: MR19- 03C, 04	Mirai	1 h	2019	2712	CO	2B, 205	1%	Yugo Kanaya	R1,2,4,5,10, 11		DOI: 10.17596/0002077, 10.17596/0002101, 10.17596/0002118
S9	MR20: MR20- E01, 05C, E02, 01	Mirai	1 h	2020	2787	CO	2B, 205	1%	Yugo Kanaya	R1,2,10		DOI: 10.17596/0002152, 10.17596/0002165, 10.17596/0002191, 10.17596/0002121
S10	MR21: MR21- 01, 03, 05C, 06	Mirai	1 h	2021	2990	CO	2B, 205	1%	Yugo Kanaya	R1,2,10		DOI: 10.17596/0002308, 10.17596/0002310, 10.17596/0002331, 10.17596/0002312, 10.17596/0002313

S11	KH-18-6	Hakuho Maru	1 h	2018	527	CO	2B, 205	1%	Yugo Kanaya	R4,5	Ueda et al. (2023)
S12	NAAMES1	Atlantis	1 h	2015	525	CN	Thermo, 49C ppb	$\pm(2 + 5\%)$	James Johnson	R7	<a href="https://saga.pmel.noaa.gov/data/">https://saga.pmel.noaa.gov/data/</a>
S13	NAAMES2	Atlantis	1 h	2016	529	CN	Thermo, 49C		James Johnson	R7	<a href="https://saga.pmel.noaa.gov/data/">https://saga.pmel.noaa.gov/data/</a>
S14	NAAMES3	Atlantis	1 h	2017	486	CN	Thermo, 49C		James Johnson	R7	<a href="https://saga.pmel.noaa.gov/data/">https://saga.pmel.noaa.gov/data/</a>
S15	NAAMES4	Atlantis	1 h	2018	497	CN	Thermo, 49C		James Johnson	R7,8	<a href="https://saga.pmel.noaa.gov/data/">https://saga.pmel.noaa.gov/data/</a>
S16	ATOMIC	Ronald H. Brown	1 h	2020	695	CN	Thermo, 49C		James Johnson	R8	<a href="https://saga.pmel.noaa.gov/data/">https://saga.pmel.noaa.gov/data/</a>
S17	DYNAMO	Roger Revelle	1 h	2011	1130	CN	Thermo, 49C		James Johnson	R4,5	<a href="https://saga.pmel.noaa.gov/data/">https://saga.pmel.noaa.gov/data/</a>
S18	WACS	Knorr	1 h	2014	192	CN	Thermo, 49C		James Johnson	R7	<a href="https://saga.pmel.noaa.gov/data/">https://saga.pmel.noaa.gov/data/</a>
S19	VOCALS	Ronald H. Brown	1 h	2008	745	CN	TECO 49		James Johnson	R2,3	<a href="https://saga.pmel.noaa.gov/data/">https://saga.pmel.noaa.gov/data/</a>
S20	MAGE92	R/V John Vickers	1 h	1992	670	CN	Dasibi 1008 AH	N/A	James Johnson	R1,2	<a href="https://saga.pmel.noaa.gov/data/">https://saga.pmel.noaa.gov/data/</a>
S21	RITS93	R/V Surveyor	1 h	1993	939	CN	Dasibi 1008 AH	N/A	James Johnson	R1,2,3,9,11	<a href="https://saga.pmel.noaa.gov/data/">https://saga.pmel.noaa.gov/data/</a>
S22	RITS94	R/V Surveyor	1 h	1994	965	CN	Dasibi 1008 AH and TECO 49	N/A	James Johnson	R1,2,3,9,11	<a href="https://saga.pmel.noaa.gov/data/">https://saga.pmel.noaa.gov/data/</a>
S23	ACE1	Discoverer	1 h	1995	1102	CN	Dasibi 1008 AH and TECO 49	N/A	James Johnson	R1,2,3	<a href="https://saga.pmel.noaa.gov/data/">https://saga.pmel.noaa.gov/data/</a>
S24	ACEASIA	Ronald H. Brown	1 h	2001	808	CN	Dasibi 1008 AH and TECO 49	N/A	James Johnson	R1	<a href="https://saga.pmel.noaa.gov/data/">https://saga.pmel.noaa.gov/data/</a>
S25	NEAQS 2002	Ronald H. Brown	1 h	2002	467	NO, NO <sub>2</sub>	Dasibi 1008 AH and TECO 49	$\pm(2\% + 1$ ppb)	<u>(Kenneth Aikin)</u>	R7	<a href="https://cs1.noaa.gov/projects/neaqs/">https://cs1.noaa.gov/projects/neaqs/</a>
S26	NEAQS 2004	Ronald H. Brown	1 h	2004	699	CO, NO, NO <sub>2</sub>	Dasibi 1008 AH and TECO 49	$\pm(2 + 5\%)$ ppb	<u>(Kenneth Aikin)</u>	R7	<a href="https://cs1.noaa.gov/projects/2004/">https://cs1.noaa.gov/projects/2004/</a>
S27	TEXAQS 2006	Ronald H. Brown	1 h	2006	604	CO, NO, NO <sub>2</sub>	TECO 49c	$\pm(3\% +$ 0.05) ppbv	<u>(Kenneth Aikin)</u>	R7	<a href="https://cs1.noaa.gov/projects/2006/">https://cs1.noaa.gov/projects/2006/</a>
S28	ICEALOT	Knorr	1 h	2008	726	CO, NO, NO <sub>2</sub> , CN_13	TECO 49c	$\pm(2\% +$ 0.05) ppbv	Kenneth Aikin and James Johnson	R7,10	<a href="https://cs1.noaa.gov/groups/cs17/measurements/2008ICEALOT/">https://cs1.noaa.gov/groups/cs17/measurements/2008ICEALOT/</a>

S29	CalNex 2010	Atlantis	1 h	2010	473	CO, NO, NO <sub>2</sub>	Thermo Environmenta 149e	± (2% + 1) ppb	<u>(Kenneth Aikin)</u>	R1	<a href="https://csl.noaa.gov/projects/calnex/">https://csl.noaa.gov/ projects/calnex/</a>
S30	MALASPINA	Hesperides	1 h	2010	3733	N/A	UV absorption / 2B-205	N/A	Alfonso Saiz- Lopez	R1,2,3,5,7,8 ,9	Prados- Roman et al. (2015)
S31	DRAKE2009	Polar Stern	1 h	2009	215	N/A	2B	N/A	<u>[#Theodore Koenig]</u>	R9	<a href="https://esr.seadatagrid.org/report/21000666">https://esr.seadatagrid.org/report/21000666</a> <sub>6</sub>
S32	MAP-IO/ SWING 2021	Marion_Dufresne	1 h	2021	938	N/A	HORIBA APOA-370	N/A	Aurélie Colomb, Pierre Tulet	R5	<a href="http://www.mapio.re/">http://www.mapio.re/</a> <a href="https://www.aeris-data.fr/catalogue-map-io/">https://www.aeris-data.fr/catalogue-map-io/</a>
S33	MAP IO/ OP1 TAAF 2021	Marion_Dufresne	1 h	2021	630	N/A	HORIBA APOA-370	N/A	Aurélie Colomb, Pierre Tulet	R4,5	<a href="http://www.mapio.re/">http://www.mapio.re/</a> <a href="https://www.aeris-data.fr/catalogue-map-io/">https://www.aeris-data.fr/catalogue-map-io/</a>
S34	MAP IO/ SCRATCH 2021	Marion_Dufresne	1 h	2021	342	N/A	HORIBA APOA-370	N/A	Aurélie Colomb, Pierre Tulet	R4,5	<a href="http://www.mapio.re/">http://www.mapio.re/</a> <a href="https://www.aeris-data.fr/catalogue-map-io/">https://www.aeris-data.fr/catalogue-map-io/</a>
S35	MAP IO/ OP2 TAAF 2021	Marion_Dufresne	1 h	2021	593	N/A	HORIBA APOA-370	N/A	Aurélie Colomb, Pierre Tulet	R4,5	<a href="http://www.mapio.re/">http://www.mapio.re/</a> <a href="https://www.aeris-data.fr/catalogue-map-io/">https://www.aeris-data.fr/catalogue-map-io/</a>
S36	MAP IO/ MAYOBS 2021	Marion_Dufresne	1 h	2021	438	N/A	HORIBA APOA-370	N/A	Aurélie Colomb, Pierre Tulet	R4,5	<a href="http://www.mapio.re/">http://www.mapio.re/</a> <a href="https://www.aeris-data.fr/catalogue-map-io/">https://www.aeris-data.fr/catalogue-map-io/</a>
S37	MAP IO/ OP3 TAAF 2021	Marion_Dufresne	1 h	2021	600	N/A	HORIBA APOA-370	N/A	Aurélie Colomb, Pierre Tulet	R5	<a href="http://www.mapio.re/">http://www.mapio.re/</a> <a href="https://www.aeris-data.fr/catalogue-map-io/">https://www.aeris-data.fr/catalogue-map-io/</a>
S38	MAP IO/ OP4 TAAF 2021	Marion_Dufresne	1 h	2021	349	N/A	HORIBA APOA-370	N/A	Aurélie Colomb, Pierre Tulet	R4,5	<a href="http://www.mapio.re/">http://www.mapio.re/</a> <a href="https://www.aeris-data.fr/catalogue-map-io/">https://www.aeris-data.fr/catalogue-map-io/</a>
S39	Ka'imimoana	R/V Ka'imimoana	1 h	2012	505	N/A		N/A	Rainer Volkamer, Theodore Koenig	R2,3	Coburn et al. (2014)

			N/A	1977-96: a wet chemical instrument using the potassium iodide (KI) method; 1995-2002: Thermo Instrument UV absorption spectrometer; 2002- Thermo Environmental 149 and 49C	R3,5,7,8,9,1 Lelieveld et al. (2004)	
S40	DWD-MPI	Meteor;Polarstern; Walther_Herwig; Anton_Dohrn;Ymer; Academie Fedorov -(DWD;1977- 1996)+ Berlin_Express (MPI;1995-2002); Meteor (MPI;2002)	1977 1 h	103352 2002	5ppb, 1995- 2002: 6%±2 ppb, 2002-<5%	<u>4</u> Theodore Koenig]
S41	17v01	Investigator	1 h	2017 1067	N/A	
S42	17v02	Investigator	1 h	2017 223	N/A	
S43	17v03	Investigator	1 h	2017 729	N/A	
S44	17v04	Investigator	1 h	2017 412	N/A	
S45	17v05	Investigator	1 h	2017 670	N/A	
S46	18v01	Investigator	1 h	2018 864	N/A	
S47	18v02	Investigator	1 h	2018 359	N/A	
S48	18v03	Investigator	1 h	2018 397	N/A	
S49	18v04	Investigator	1 h	2018 588	N/A	
						<a href="https://data.csiro.au/">https://data.csiro.au/</a> (Data will be available in 2025)

S50	18v05	Investigator	1 h	2018	657	N/A	Thermo Scientific 49i analyser $\times 2$	Suzie Molloy	R3	
S51	18v06	Investigator	1 h	2018	581	N/A	Thermo Scientific 49i analyser $\times 2$	Suzie Molloy	R3	
S52	18v08	Investigator	1 h	2018	284	N/A	Thermo Scientific 49i analyser $\times 2$	Suzie Molloy	R3	
S53	19v01	Investigator	1 h	2019	848	N/A	Thermo Scientific 49i analyser $\times 2$	Suzie Molloy	R3,11	
S54	19v02	Investigator	1 h	2019	425	N/A	Thermo Scientific 49i analyser $\times 2$	Suzie Molloy	R3	
S55	19v03	Investigator	1 h	2019	667	N/A	Thermo Scientific 49i analyser $\times 2$	Suzie Molloy	R2,3,5	
S56	IIOE2	R/V Sagar Nidhi	1 h	2015	211	N/A	Ecotech EC9810B	1 ppbv	Anoop Mahajan	R4,5
S57	SOE9	S A Agulhas	1 h	2016	1121	N/A	Ecotech EC9810B	1 ppbv	Anoop Mahajan	R5,11
S58	SOE11	S A Agulhas	1 h	2020	824	N/A	Ecotech EC9810B	1 ppbv	Anoop Mahajan	R5,11
B1	O-Buoy01	O-Buoy	1 h	2009 – 2010	4741	N/A	2B Technologies, custom-built model 205 dual-beam <del>O<sub>3</sub></del> <ins>O<sub>3</sub> + O<sub>2</sub></ins> monitors	John W Halfacre and individual measurement uncertainty was calculated to range from 2.1 to 1 <del>ppbv</del> <ins>ppb</ins>	R10	
B2	O-Buoy02	O-Buoy	1 h	2010 – 2011	2832	N/A		John W Halfacre	R10	Halfacre et al. (2014)
B3	O-Buoy03	O-Buoy	1 h	2010 – 2011	1405	N/A		John W Halfacre	R10	
B4	O-Buoy04	O-Buoy	1 h	2010 – 2012	4424	N/A		John W Halfacre	R10	

B5	O-Buoy05	O-Buoy	1 h	2011 — 2012	N/A 1036		John W Halfacre	R10
B6	O-Buoy06	O-Buoy	1 h	2012	338		John W Halfacre	R10
B7	O-Buoy07	O-Buoy	1 h	2012 — 2013	N/A 955		John W Halfacre	R10
B8	O-Buoy08	O-Buoy	1 h	2012 — 2016	N/A 2823		John W Halfacre	R10
B9	O-Buoy09	O-Buoy	1 h	2013	46		John W Halfacre	R10
B10	O-Buoy10	O-Buoy	1 h	2013 — 2014	N/A 3777		John W Halfacre	R10
B11	O-Buoy11	O-Buoy	1 h	2014	N/A 3338		John W Halfacre	R10
B12	O-Buoy12	O-Buoy	1 h	2014 — 2015	N/A 851		John W Halfacre	R10
B13	O-Buoy13	O-Buoy	1 h	2015	N/A 1881		John W Halfacre	R10
B14	O-Buoy14	O-Buoy	1 h	2015 — 2017	N/A 6229		John W Halfacre	R10
B15	O-Buoy15	O-Buoy	1 h	2015 — 2016	N/A 389		John W Halfacre	R10
S59	YES-AQ	R/V Gisang I	1 h	2015 — 2021	N/A 2156	Thermo, Model 49C	Junsoo Gil	R1 <u>Ahn et al. (2024)</u>
S60	MOSAiC	R/V Polarstern	1 h	2019 — 2020	8131	Thermo Fisher Scientific 49i/9c, 2B Technologies 205	Julia Schmale	R10 Angot et al. (2022)
S61	SAGA3	R/V Korolev	1 h	1990	562	N/A 1008-AH	Dabibi model ± 3 ppbv James Johnson	R8 Thompson et al. (1993)
								<a href="https://doi.pangaea.de/10.1594/PANGAE/A.944393">https://doi.pangaea.de/10.1594/PANGAE/A.944393</a> <a href="https://doi.pangaea.de/10.1594/PANGAE/A.944389">https://doi.pangaea.de/10.1594/PANGAE/A.944389</a>
								<a href="https://saga.pmel.noaa.gov/data/">https://saga.pmel.noaa.gov/data/</a>

S62	AEROSOLS99-INDOEX	Ronald H. Brown	1 h	1999	1392	CN	Dasibi 1008 AH and TECO 49	N/A	James Johnson	R4,5,7,8,9	<a href="https://saga.pmel.noaa.gov/data/">https://saga.pmel.noaa.gov/data/</a>
-----	-------------------	-----------------	-----	------	------	----	----------------------------------	-----	---------------	------------	---

**Table 2.** List of aircraft-based campaign data contained in the aircraft data-set.

Label	Campaign	Platform	Resolution	Year	Data number <2000m	Ancillary data	Instrument	Uncertainty	PIC Data Manager-[ <a href="#">WG member worked on the data</a> ]	Regions	Literature	Data source	
A1	ABLE-2B	Electra	60 s	1987	67	677	CO	N/A	<a href="#">(Gao Chen)</a>	R7,8	Harriss et al. (1990)	<a href="https://www-gte.larc.nasa.gov/gte_mrg1.htm#ABLE-2B">https://www-gte.larc.nasa.gov/gte_mrg1.htm#ABLE-2B</a>	
A2	ABLE-3A	Electra	60 s	1988	1668	3824	NO	N/A	<a href="#">(Gao Chen)</a>	R1,7,10	Harriss et al. (1992)	<a href="https://www-gte.larc.nasa.gov/gte_mrg1.htm#ABLE-3A">https://www-gte.larc.nasa.gov/gte_mrg1.htm#ABLE-3A</a>	
A3	ABLE-3B	Electra	90 s	1990	133	258	CO, NO, NO <sub>2</sub>	N/A	<a href="#">(Gao Chen)</a>	R7,10	Harriss et al. (1994)	<a href="https://www-gte.larc.nasa.gov/gte_mrg1.htm#ABLE-3B">https://www-gte.larc.nasa.gov/gte_mrg1.htm#ABLE-3B</a>	
A4	CITE-3	Electra	10 s	1989	21355	28718	CO	<del>Chemiluminescence</del> <u>Chemiluminescence</u>	<a href="#">(Gao Chen)</a>	R7,8	Hoell Jr. et al. (1993)	<a href="https://www-gte.larc.nasa.gov/gte_mrg1.htm#CITE-3">https://www-gte.larc.nasa.gov/gte_mrg1.htm#CITE-3</a>	
A5	PEM-West A	DC-8	90 s	1991	801	1511	CO, NO, NO <sub>2</sub>	5% or 2ppb	<a href="#">(Gao Chen)</a>	R1,2	Hoell et al. (1996)	<a href="https://www-gte.larc.nasa.gov/gte_mrg1.htm#PEM%20W">https://www-gte.larc.nasa.gov/gte_mrg1.htm#PEM%20W</a>	
A6	PEM-West B	DC-8	30 s	1994	2142	5259	CO, NO	Chemiluminescene	3% or 2ppb	<a href="#">(Gao Chen)</a>	R1,2	Hoell et al. (1997)	<a href="https://www-gte.larc.nasa.gov/gte_mrg1.htm#PEM%20W">https://www-gte.larc.nasa.gov/gte_mrg1.htm#PEM%20W</a>
A7	TRACE-A	DC-8	90 s	1992	131	408	CO, NO, NO <sub>2</sub>	N/A	<a href="#">(Gao Chen)</a>	R5,7,8,9	Fishman et al. (1996)	<a href="https://www-gte.larc.nasa.gov/gte_mrg1.htm#TRACE-A">https://www-gte.larc.nasa.gov/gte_mrg1.htm#TRACE-A</a>	
A8	PEM-Tropics A	DC-8	60 s	1996	1395	2969	CO, NO, NO <sub>2</sub>	Chemilumi nescene	3% or 2ppb	<a href="#">(Gao Chen)</a>	R1,2,3,1	Hoell et al. (1999)	<a href="https://www-gte.larc.nasa.gov/gte_mrg1.htm#PEM%20TROPICS-A">https://www-gte.larc.nasa.gov/gte_mrg1.htm#PEM%20TROPICS-A</a>

A9	PEM-Tropics B P3B	P3B	60 s	1999	3111	4939	CO, NO, NO <sub>2</sub>	Chemilumi nescence	3% or 2 ppb	<a href="#">(Gao Chen)</a>	R1,2,3,7	<a href="#">Paper et al. (2001)</a>	<a href="https://www-gte.larc.nasa.gov/gte_mrg1.htm#PEM%20TROPICS-B">https://www-gte.larc.nasa.gov/gte_mrg1.htm#PEM%20TROPICS-B</a>
A10	PEM-Tropics B DC8	DC-8	60 s	1999	1573	3027	CO, NO, NO <sub>2</sub>	Chemilumi nescence	3% or 2 ppb	<a href="#">(Gao Chen)</a>	R1,2,3,8		
A11	TRACE-P P3B	P3B	60 s	2001	3036	6374	CO, NO, NO <sub>2</sub>	Chemilumi nescence	5% or 2 ppb	<a href="#">(Gao Chen)</a>	R1,2,7	<a href="#">Jacob et al. (2003)</a>	<a href="https://www-gte.larc.nasa.gov/gte_mrg1.htm#TRACE-P">https://www-gte.larc.nasa.gov/gte_mrg1.htm#TRACE-P</a>
A12	TRACE-P DC8	DC-8	60 s	2001	2024	3925	CO, NO, NO <sub>2</sub>	Chemilumi nescence	5% or 2 ppb	<a href="#">(Gao Chen)</a>	R1,2	<a href="#">Singh et al. (2006)</a>	<a href="https://www-air.larc.nasa.gov/missions/intexna.htm">https://www-air.larc.nasa.gov/missions/intexna.htm</a>
A13	INTEX-NA	DC-8	60 s	2004	1056	1739	CO, NO, NO <sub>2</sub>	Chemilumi nescence	5% or 1 ppb	<a href="#">(Gao Chen)</a>	R1,7		<a href="https://www-air.larc.nasa.gov/missions/intexb.htm">https://www-air.larc.nasa.gov/missions/intexb.htm</a>
A14	INTEX-B DC8	DC-8	60 s	2006	1262	2695	CO, NO, NO <sub>2</sub>	Chemilumi nescence	1 ppb or 5%	<a href="#">(Gao Chen)</a>	R1,2,7	<a href="#">Singh et al. (2009)</a>	<a href="https://www-air.larc.nasa.gov/missions/intexb.htm">https://www-air.larc.nasa.gov/missions/intexb.htm</a>
A15	INTEX-B C-130	C-130	60 s	2006	741	2468	CO, NO, NO <sub>2</sub>	Chemilumi nescence	0.1 ppbv or 5%	<a href="#">(Gao Chen)</a>	R1,2,7	<a href="#">Shon et al. (2008), Kleib et al. (2011)</a>	<a href="https://www-llnl.gov/field_projects/millagro">https://www-llnl.gov/field_projects/millagro</a>
A16	ARCTAS	DC-8	60 s	2008	1287	2444	CO, NO, NO <sub>2</sub>	Chemilumi nescence	±2 ppbv	Andrew Weinheimer, Denise Montska, David Knapp, and Ilana Pollack	R1,10	<a href="#">Jacob et al. (2010)</a>	<a href="https://www-air.larc.nasa.gov/cgi-bin/ArcView/arctas">https://www-air.larc.nasa.gov/cgi-bin/ArcView/arctas</a>
A17	SEAC4RS DC8	DC-8	60 s	2013	376	601	CO, NO, NO <sub>2</sub>	<del>Chemilumi nescence</del> <del>CO, NO, NO<sub>2</sub></del> <del>Chemilumi nescence</del>	0.030 ppbv + 3%	Tom Ryerson, Jeff Peischl and Ilana Pollack	R1,7		<a href="https://www-air.larc.nasa.gov/cgi-bin/ArcView/seac4rs">https://www-air.larc.nasa.gov/cgi-bin/ArcView/seac4rs</a>
A18	SEAC4RS ER2	ER2	60 s	2013	83	202	CO	UV absorption	3% precision	<a href="#">(Gao Chen)</a>	R7		<a href="https://www-air.larc.nasa.gov/cgi-bin/ArcView/seac4rs">https://www-air.larc.nasa.gov/cgi-bin/ArcView/seac4rs</a>

A19	DISCOVER-AQ	P3B	60 s	2013	145	162	NO, NO <sub>2</sub>	4ch chemiluminescence	0.1 ppbv + 5%	<a href="https://www-air.larc.nasa.gov/cgi-bin/ArcView/discover-aq.cgi?2014/P3B=1">https://www-air.larc.nasa.gov/cgi-bin/ArcView/discover-aq.cgi?2014/P3B=1</a>
A20	KORUS-AQ	DC-8	60 s	2016	2057	2631	CO, NO, NO <sub>2</sub>	4ch chemiluminescence	5 ppbv + 10%	<a href="https://www-air.larc.nasa.gov/cgi-bin/ArcView/korusaq">https://www-air.larc.nasa.gov/cgi-bin/ArcView/korusaq</a>
A21	ATom1-4	DC-8	10 s	2016–2018	23715	42975	CO, NO, NO <sub>2</sub>	4ch chemiluminescence	5–10 ppt	<a href="https://daac.ornl.gov/cgi-bin/dsviewer.pl?ds_id=1581">https://daac.ornl.gov/cgi-bin/dsviewer.pl?ds_id=1581</a>
A22	HIPPO	NSF NCAR G-V	10 s	2009–2011	20509	45018	CO	Ultraviolet absorption	Final data. Accuracy approximately ±5%	<a href="https://www-eo.llnl.gov/projects/hippo">https://www-eo.llnl.gov/projects/hippo</a>
A23	ACESIS FAAM	FAAM/BAE-146-301	10 s	2017–2020	23046	34840	CO	TECO 49	N/A	<a href="https://catalogue.ceda.ac.uk/uu_id/8df2e81dbfc2499983aa87781fb3fd15a/">https://catalogue.ceda.ac.uk/uu_id/8df2e81dbfc2499983aa87781fb3fd15a/</a>
A24	ACCACIA FAAM	FAAM/BAE-146-301	10 s	2013	7548	11369	CO		James Lee	<a href="https://www-faam.ac.uk/sphinx/coredata/dynamical_content/modules.html#t ozone">https://www-faam.ac.uk/sphinx/coredata/dynamical_content/modules.html#t ozone</a>
A25	CAST FAAM	FAAM/BAE-146-301	10 s	2014	7210	10566	CO		James Lee	R1
A26	CLARIFY FAAM	FAAM/BAE-146-301	10 s	2017	14248	24319	CO		James Lee	R8

A27	ITOP FAAM	FAAM/ BAE-146-301	10 s	2004	4683	13350	CO			James Lee	R7	
A28	VOCALS FAAM	FAAM/ BAE-146-301	10 s	2008	19037	19736	CO			James Lee	R2,3	
A29	NARE1996	NOAA P-3	10 s	1996	3006	4783	CO, NO, NO <sub>2</sub>	N/A		<sup>(J)Kenneth Aikin</sup> <sub>J</sub>	R7	
A30	NARE1997	NOAA P-3	10 s	1997	4886	9931	CO, NO, NO <sub>2</sub>	N/A		<sup>(J)Kenneth Aikin</sup> <sub>J</sub>	R7	
A31	TEXAQS2000	NCAR Electra	10 s	2000	2496	3904	CO, NO, NO <sub>2</sub>	<del>Chemiluminescence</del> <del>Resonance Raman</del> <del>C hemilumin</del> <del>escence</del>	N/A	<sup>(J)Kenneth Aikin</sup> <sub>J</sub>	R7	Ryerson et al. (1998)
A32	ITCT2002	NOAA WP-3D	10 s	2002	6004	13772	CO, NO, NO <sub>2</sub>	<del>Chemiluminescence</del> <del>Resonance Raman</del> <del>C hemilumin</del> <del>escence</del>	$\pm 2\%$	<sup>(J)Kenneth Aikin</sup> <sub>J</sub>	R1,7	<a href="https://csl.noaa.gov/projects/itct2k/">https://csl.noaa.gov/projects/itct2k/</a>
A33	ITCT2004	NOAA WP-3D	10 s	2004	15213	19791	CO, NO, NO <sub>2</sub>	Chemilumi nescence	0.1 + 3%	<sup>(J)Kenneth Aikin</sup> <sub>J</sub>	R7	<a href="https://csl.noaa.gov/projects/itct2004/">https://csl.noaa.gov/projects/itct2004/</a>
A34	HURRICANE2 006	NOAA G-4	10 s	2006	334	663	none	N/A		<sup>(J)Kenneth Aikin</sup> <sub>J</sub>	R7,8	<a href="https://csl.noaa.gov/groups/csl7/measurementss/2006Hurricane2/">https://csl.noaa.gov/groups/csl7/measurementss/2006Hurricane2/</a>
A35	TEXAQS2006	NOAA WP-3D	10 s	2006	5395	6772	CO, NO, NO <sub>2</sub>	Chemilumi nescence	0.050 ppbv + 3%	<sup>(J)Kenneth Aikin</sup> <sub>J</sub>	R7	<a href="https://csl.noaa.gov/projects/2006/">https://csl.noaa.gov/projects/2006/</a>
A36	ARCPAC2008	NOAA WP-3D	10 s	2008	4878	11563	CO, NO, NO <sub>2</sub>	Chemilumi nescence	0.05 + 4%	<sup>(J)Kenneth Aikin</sup> <sub>J</sub>	R10	<a href="https://csl.noaa.gov/projects/arcpac/">https://csl.noaa.gov/projects/arcpac/</a>
A37	CalNex2010	NOAA WP-3D	10 s	2010	7040	9265	CO, NO, NO <sub>2</sub>	Chemilumi nescence	0.015 ppbv + 2%	<sup>(J)Kenneth Aikin</sup> <sub>J</sub>	R1,7	<a href="https://csl.noaa.gov/projects/calnrex/">https://csl.noaa.gov/projects/calnrex/</a>
A38	WINTERSTO RMS2001	NA	10 s	2001	164	895	none	N/A		<sup>(J)Kenneth Aikin</sup> <sub>J</sub>	R1	
A39	WINTERSTO RMS2002	NA	10 s	2002	815	1867	none	N/A		<sup>(J)Kenneth Aikin</sup> <sub>J</sub>	R1,7	
A40	WINTERSTO RMS2003	NOAA G-4	10 s	2003	657	2225	none	N/A		<sup>(J)Kenneth Aikin</sup> <sub>J</sub>	R1,7	<a href="https://csl.noaa.gov/groups/csl7/measurement">https://csl.noaa.gov/groups/csl7/measurement</a>

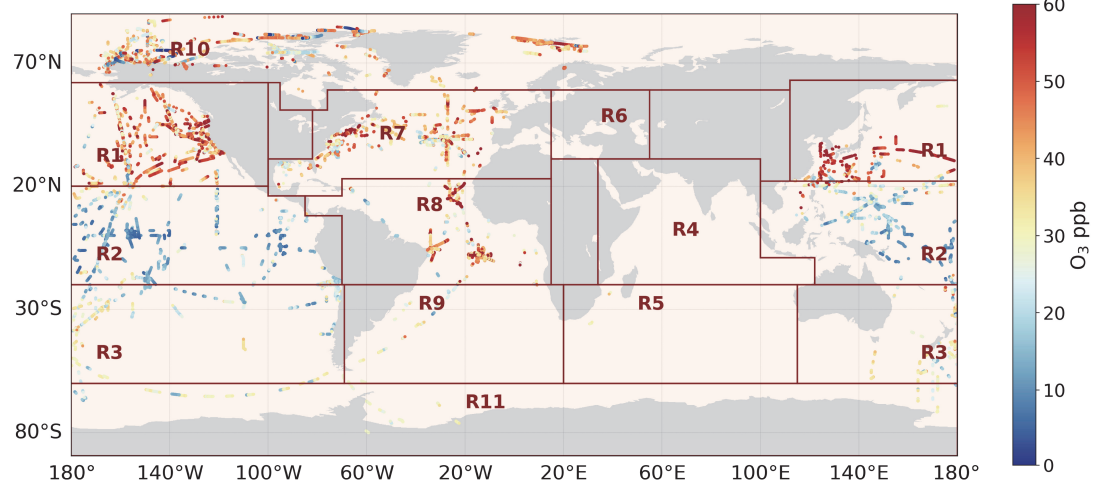
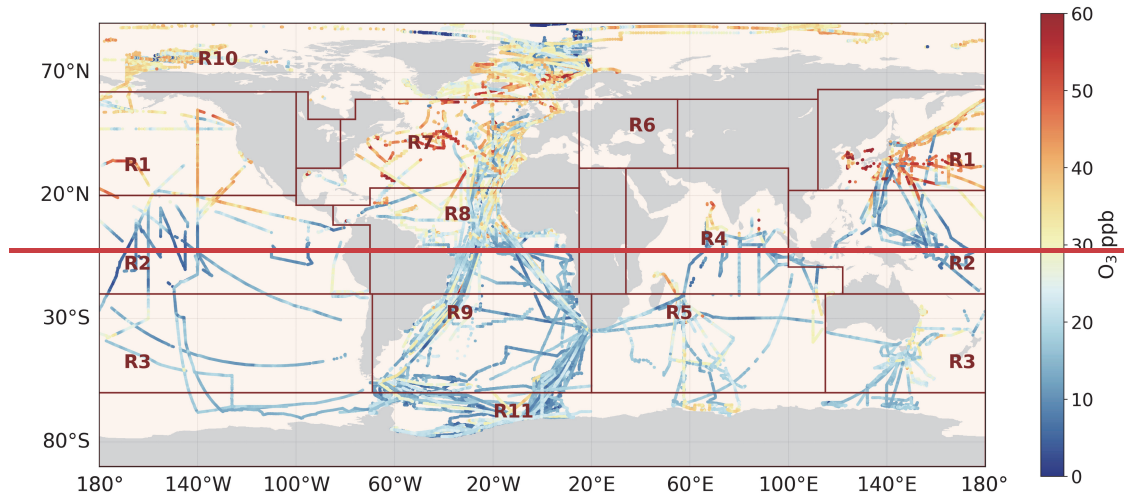
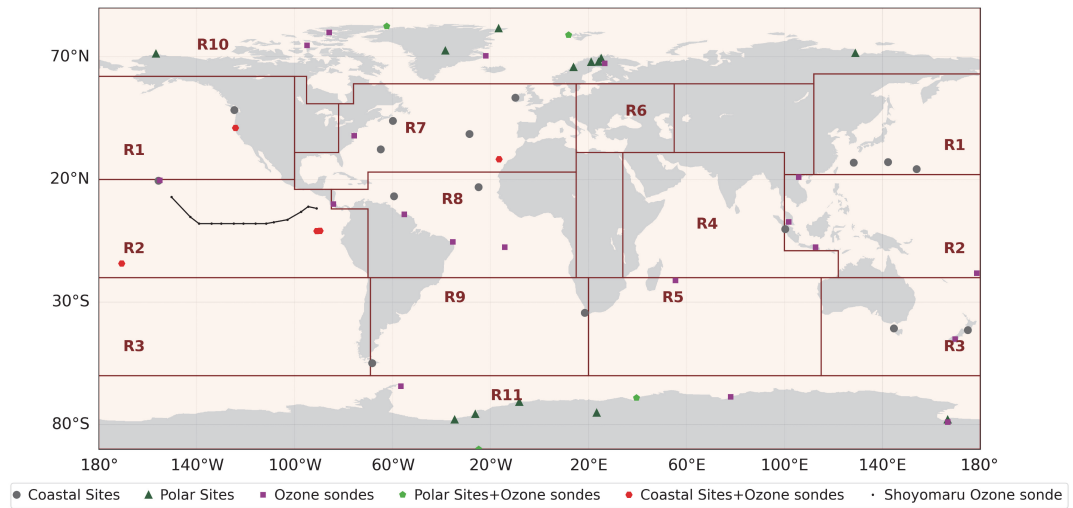
A41	WINTERSTO RMS2004	NOAA G-4	10 s	2004	992	3283	none	N/A	N/A	<a href="#">Kenneth Aikin</a> <sup>1</sup>	R1,2,7		<a href="https://open.ca/ada.ca/data/en/dataset/114347-2d-6c73-4b5c-bc2b-">https://open.ca/ada.ca/data/en/dataset/114347-2d-6c73-4b5c-bc2b-</a>
A42	WINTERSTO RMS2005	NOAA G-4	10 s	2005	541	2099	none	N/A	N/A	<a href="#">Kenneth Aikin</a> <sup>1</sup>	R1		<a href="https://csl.noaa.gov/groups/csl/7/measurement/s/2004WinterStorms/">https://csl.noaa.gov/groups/csl/7/measurement/s/2004WinterStorms/</a>
A43	WINTERSTO RMS2006	NOAA G-4	10 s	2006	900	1633	none	N/A	N/A	<a href="#">Kenneth Aikin</a> <sup>1</sup>	R1		<a href="https://csl.noaa.gov/groups/csl/7/measurement/s/2005WinterStorms/">https://csl.noaa.gov/groups/csl/7/measurement/s/2005WinterStorms/</a>
A44	WINTERSTO RMS2007	NOAA G-4	10 s	2007	355	1375	none	N/A	N/A	<a href="#">Kenneth Aikin</a> <sup>1</sup>	R1,7		<a href="https://csl.noaa.gov/groups/csl/7/measurement/s/2006WinterStorms/">https://csl.noaa.gov/groups/csl/7/measurement/s/2006WinterStorms/</a>
A45	ACTIVATE	Falcon	60 s	2020	5983	6797	CO	UV absorption	greater of $\pm 5$ ppbv or $\pm 5\%$	<a href="#">Gao Chen</a> <sup>1</sup>	R7		<a href="https://www-air.larc.nasa.gov/cgi-bin/ArcView/active/2022/HU25-1">https://www-air.larc.nasa.gov/cgi-bin/ArcView/active/2022/HU25-1</a>
A46	CONTRAST	NSF NCAR G-V	10 s	2014	3308	6318	CO, NO, NO <sub>2</sub>	Chemilumi nescence	N/A	Rainer Volkamer	R1,2	Pan et al. (2017)	<a href="https://www.eol.ucar.edu/field_projects/contrast">https://www.eol.ucar.edu/field_projects/contrast</a>
A47	TORERO	NSF NCAR G-V	10 s	2012	7129	12569	CO	<sup>Q3</sup> Dual- channel UV absorption spectrometer	<sup>3%</sup> + precision	Rainer Volkamer	R2,3,8	Volkamer et al. (2015)	<a href="https://www.eol.ucar.edu/field_projects/torero">https://www.eol.ucar.edu/field_projects/torero</a>
A48	NETCARE	Polar 6	10 s	2014– 2015	17551	27496	none	Thermo Scientific Model 49i	N/A	Ralf Staebler	R10	Abbatt et al. (2019)	<a href="https://open.ca/ada.ca/data/en/dataset/114347-2d-6c73-4b5c-bc2b-">https://open.ca/ada.ca/data/en/dataset/114347-2d-6c73-4b5c-bc2b-</a>

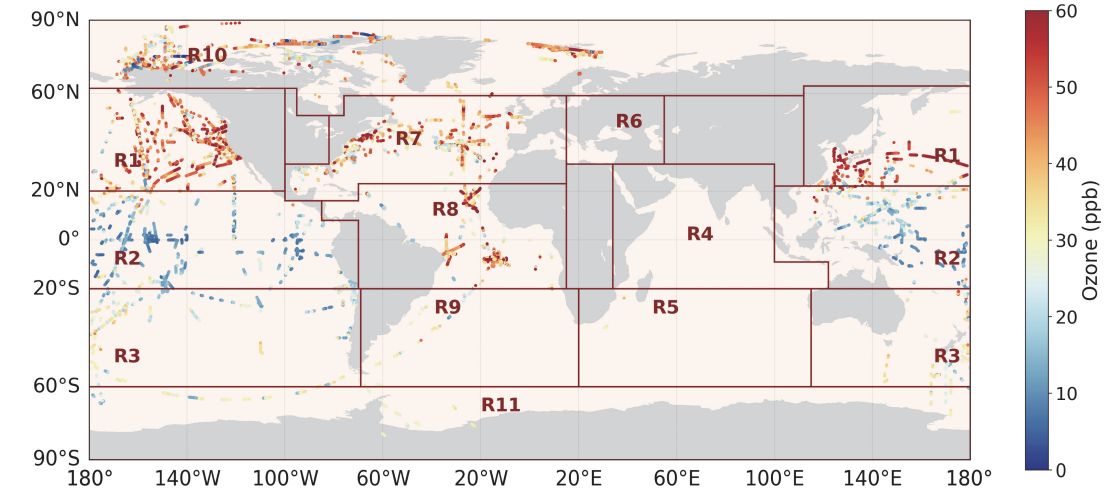
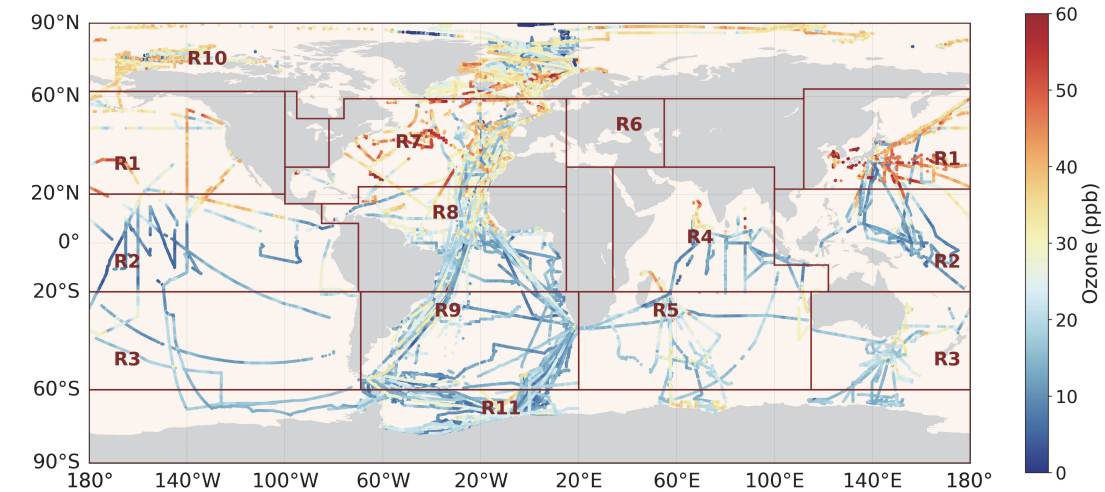
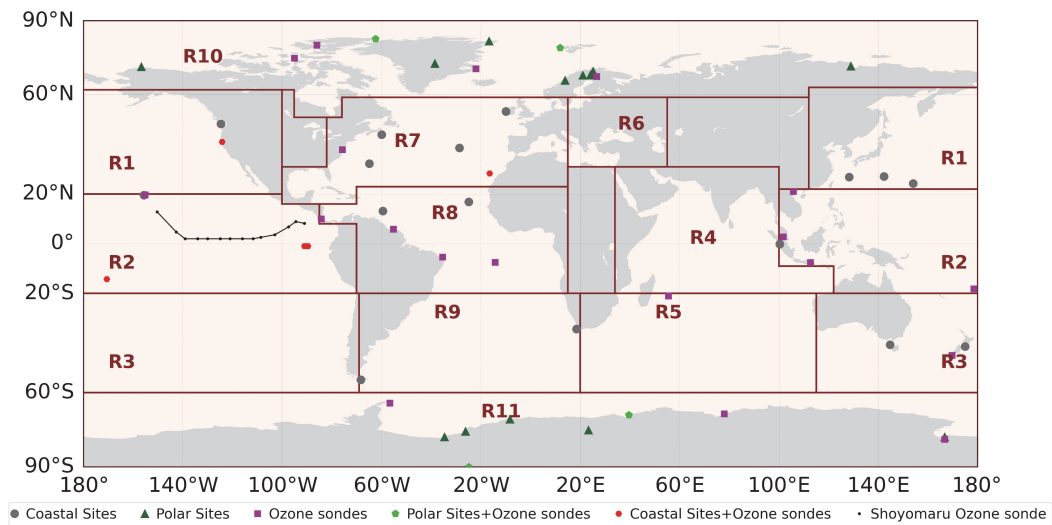
												a3d5319961e9	
												https://open.can	
												ada.ca/data/en/	
												dataset/e0e41	
												c-890d-404d-	
												bb1b-	
												221456022d51	

**Table 3.** Statistics of hourly data from the ship/buoy dataset per defined regions (R1–R11).

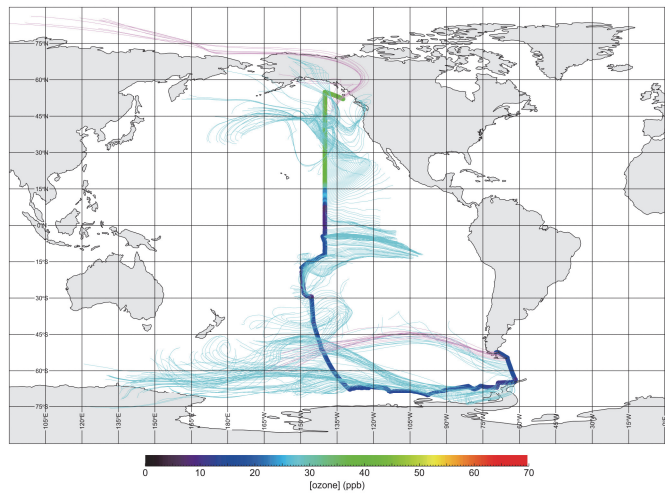
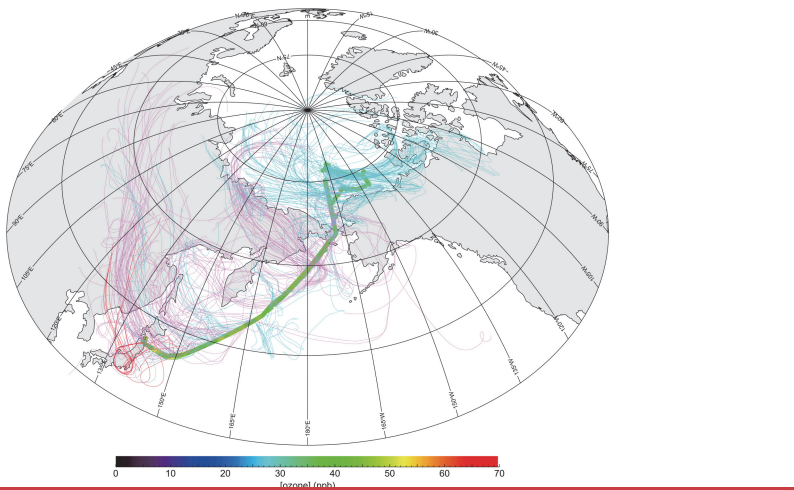
Regions	Number of hourly data (satisfying LCL72)	Maximum of hourly medians (ppb)	Local Time (hour) of maximum	Minimum of hourly medians (ppb)	Local Time (hour) of minimum	Average of 24 hourly medians (ppb)	Amplitude (max-min) (ppb)	Percentage amplitude (max-min)/average (%)
R1	6572	34.3	5	31.2	20	32.9	3.1	9.4
R2	9708	14.6	1	12.9	15	13.8	1.7	12.3
R3	6432	20.7	1, 4	19.5	14	20.1	1.2	5.7
R4	3446	17.3	3	14.7	16	16.2	2.6	16.0
R5	5651	20.0	8	19.2	0	19.7	0.9	4.4
R7	14777	32.5	1, 3, 4	30.5	14	31.6	2.0	6.5
R8	18818	21.3	5	19.0	15	20.0	2.3	11.3
R9	13710	16.0	4	15.0	15,16	15.4	1.0	6.5
R10	61708	27.5	11	25.8	8,13	26.2	1.7	6.5
R11	20215	16.0	0-7, 16-23	15.5	13	15.9	0.5	3.3



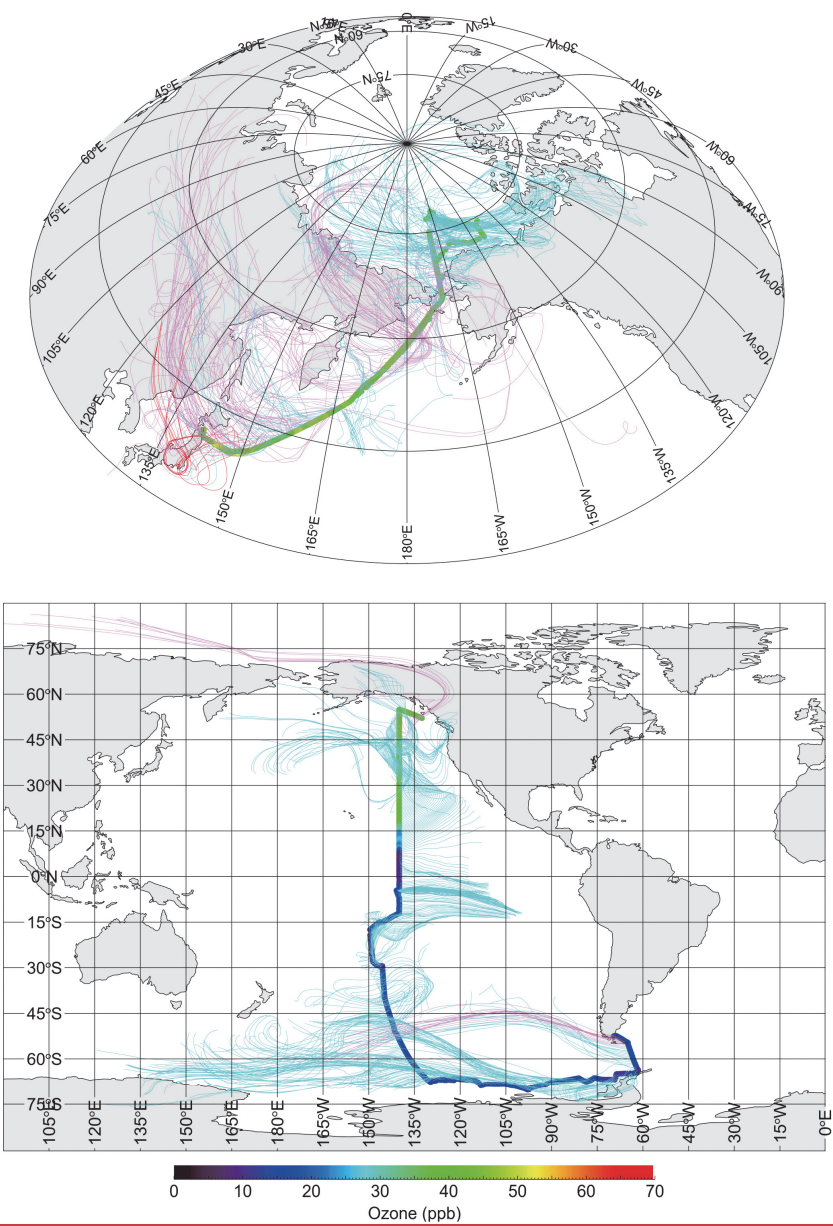




**Figure 1.** Locations of ozonesonde and coastal/polar ground observations (top). Overall ship/buoy (middle), and airborne with altitudes < 2000 m (bottom) ozone data after filtering for LCL $\geq$ 72 h. Ozone levels above 60 ppb cut off for clarity.

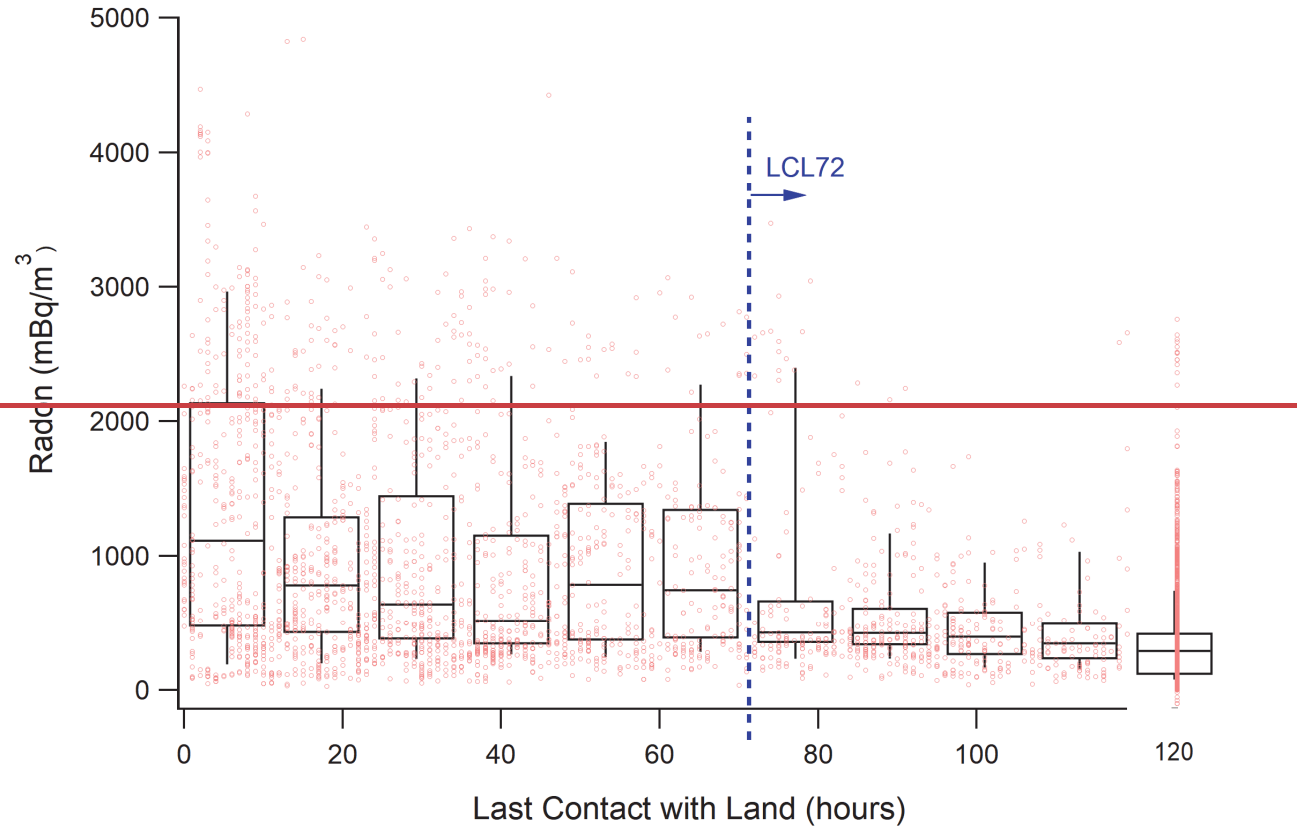


805



**Figure 2.** Backward trajectories (120-h long) for observations with oceanic conditions (light blue) and apparently land-influencing (purple) conditions, as assessed with the LCL72 criterion during (top) the MR19-03C observations from 29 Sep 2019 to 10 Nov 2019 and (bottom) the RITS94 observations from 23 Nov 1993 to 6 Jan 1994. The red lines indicate cases where the observed  $O_3$ -ozone mixing ratio is greater than 50 ppb.

810



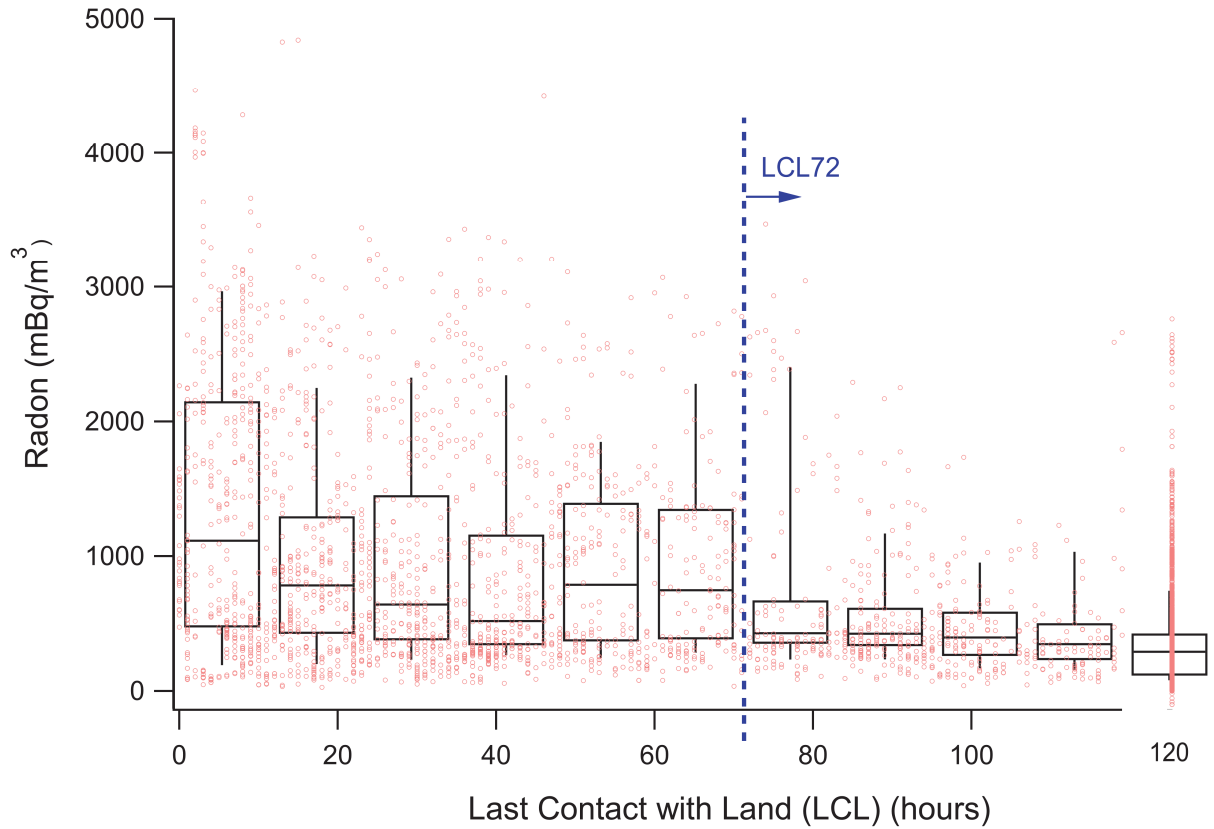
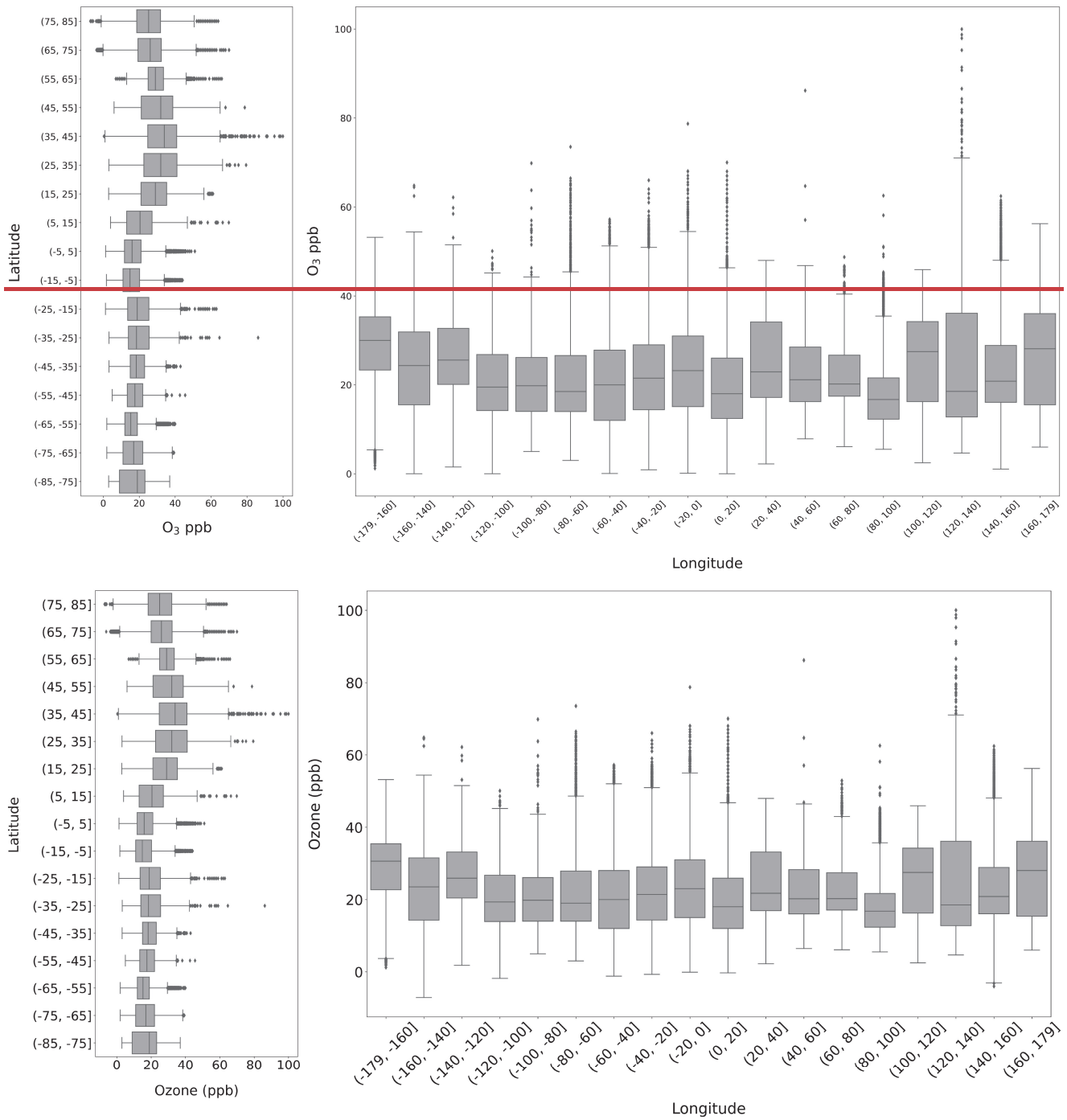


**Figure 3.** Decrease of Radon concentrations with Last Contact with Land from backward trajectory analysis. ACE-1, ACE-

815 Asia, ATOMIC, ICEALOT, NAAMES1-4, and WACS data were used in combination. Radon data by NOAA PMEL. The  
model was run with the following parameters:  $\lambda = 0.0001$ ,  $h = 1$ ,  $n = 10$ ,  $L = 100$ ,  $R = 100$ ,  $T = 100$ ,  $S = 100$ ,  $D = 100$ ,  $C = 100$ ,  $F = 100$ ,  $G = 100$ ,  $H = 100$ ,  $I = 100$ ,  $J = 100$ ,  $K = 100$ ,  $L = 100$ ,  $M = 100$ ,  $N = 100$ ,  $O = 100$ ,  $P = 100$ ,  $Q = 100$ ,  $R = 100$ ,  $S = 100$ ,  $T = 100$ ,  $U = 100$ ,  $V = 100$ ,  $W = 100$ ,  $X = 100$ ,  $Y = 100$ ,  $Z = 100$ .

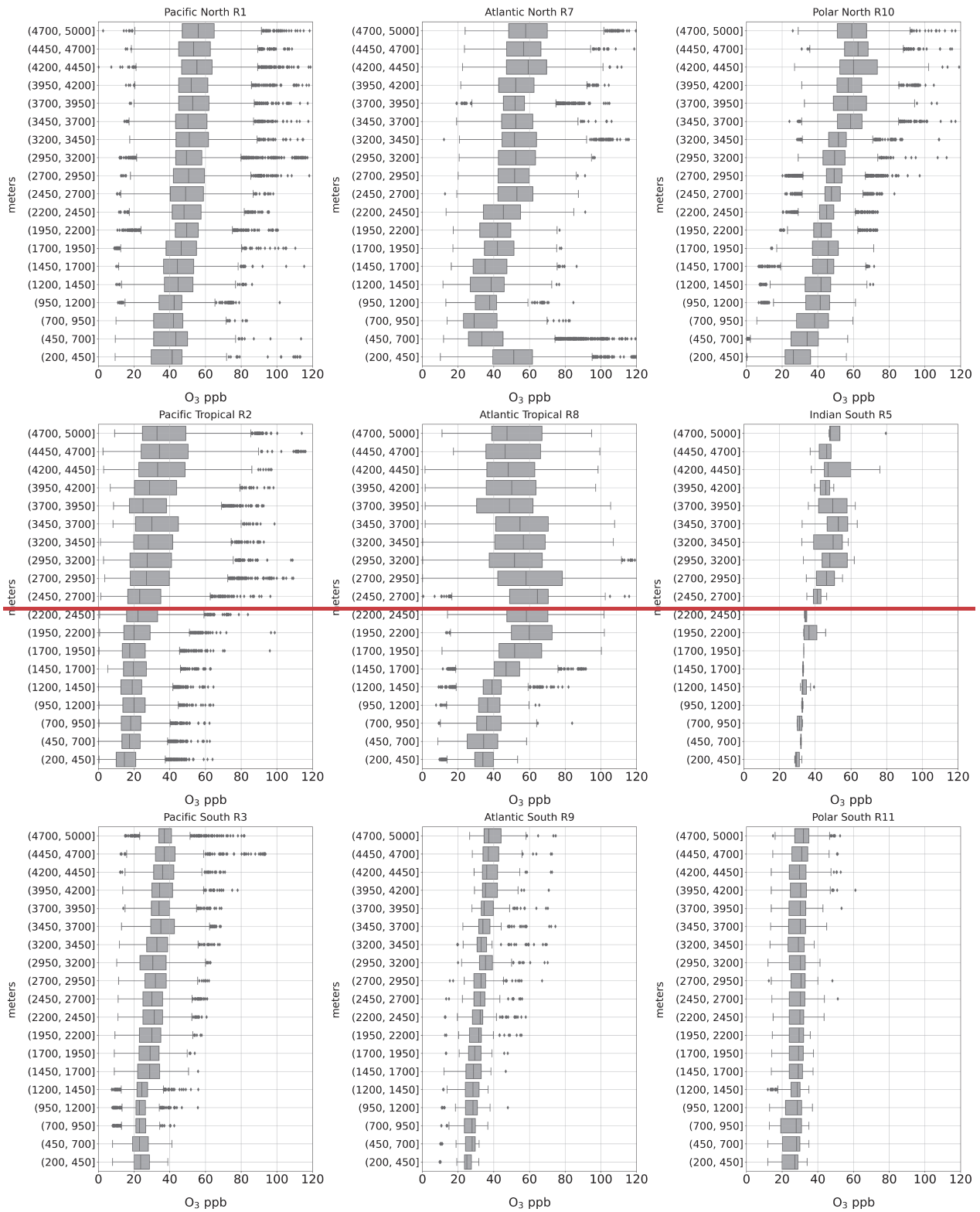


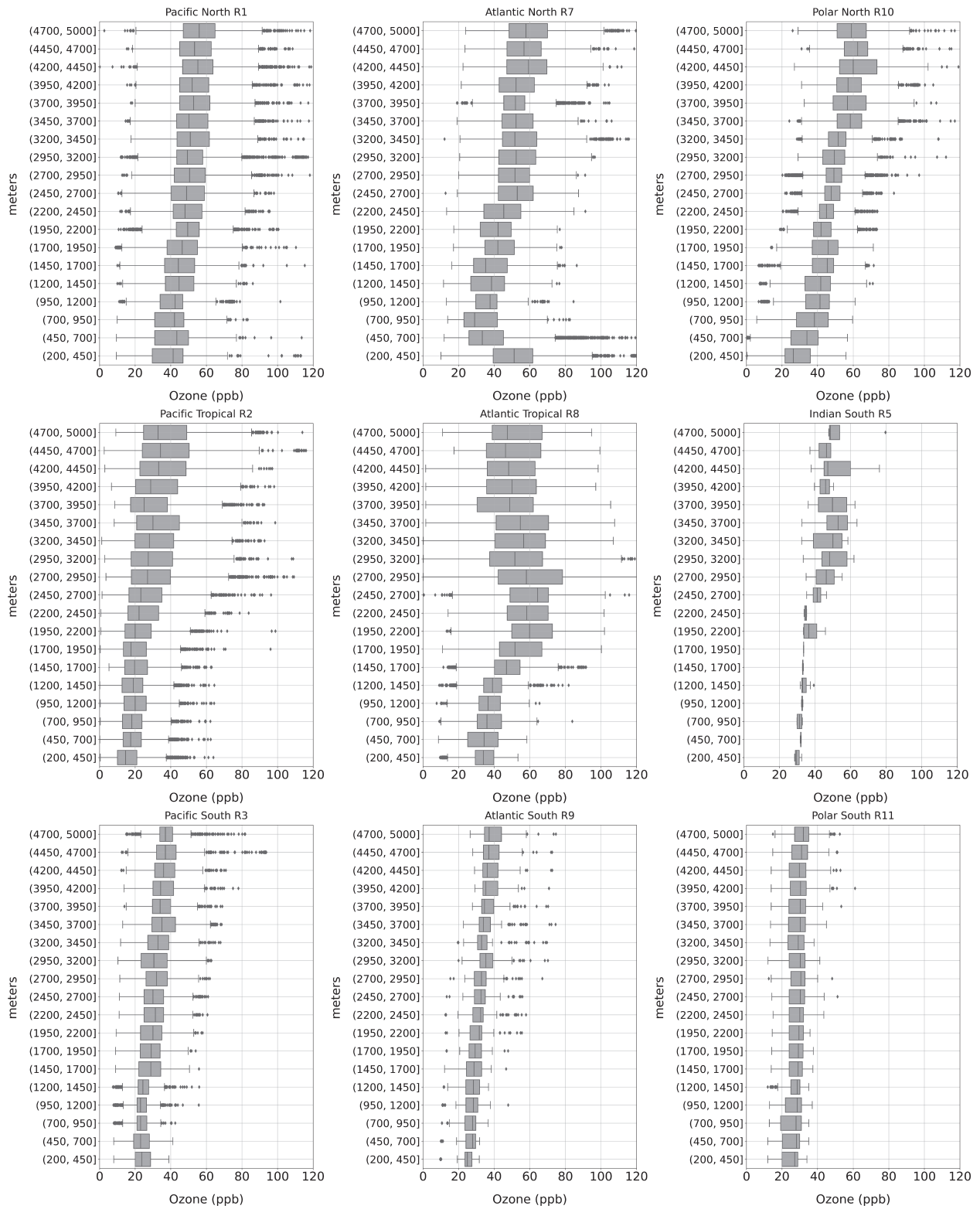
820

**Figure 4.** Latitudinal and longitudinal transect of the ship/buoy datasets, after filtering for  $LCL \geq 72$  h.



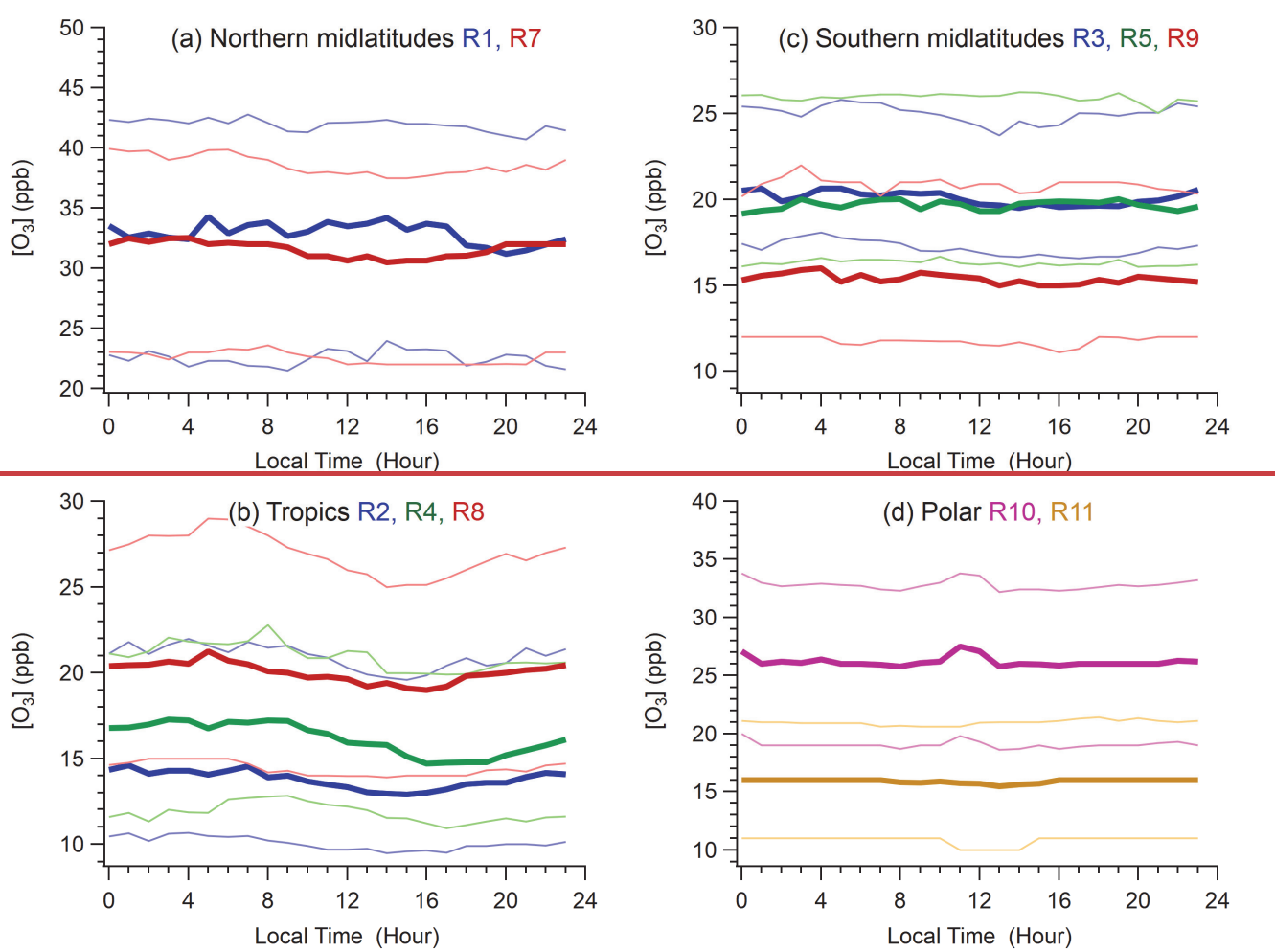


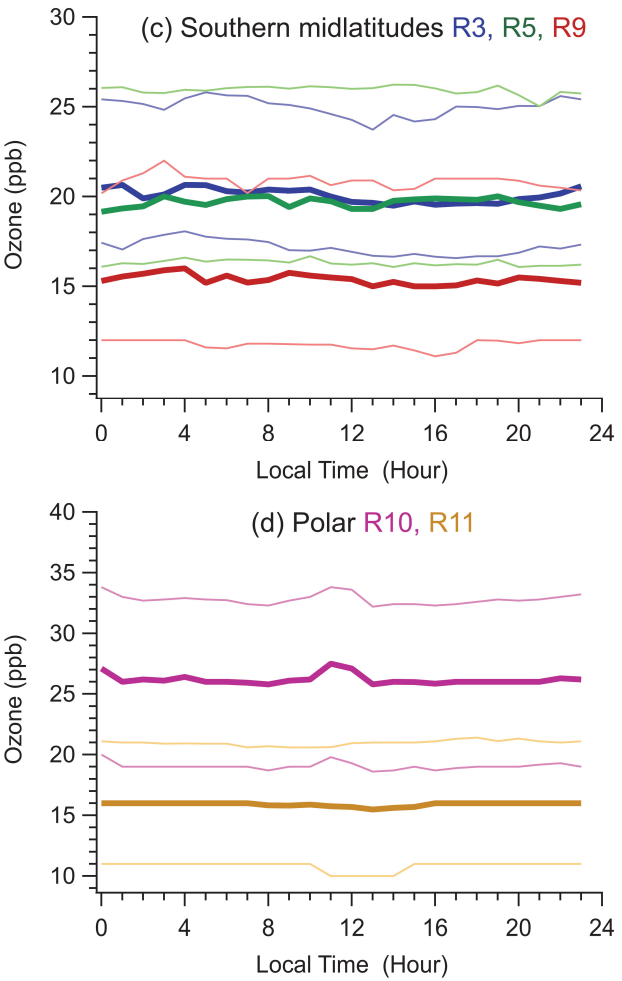
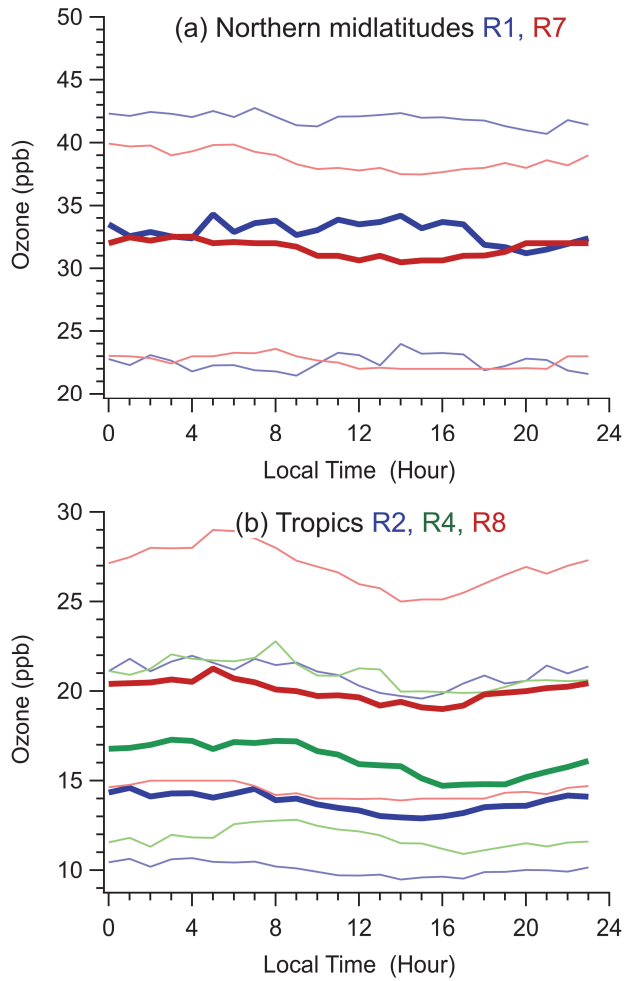




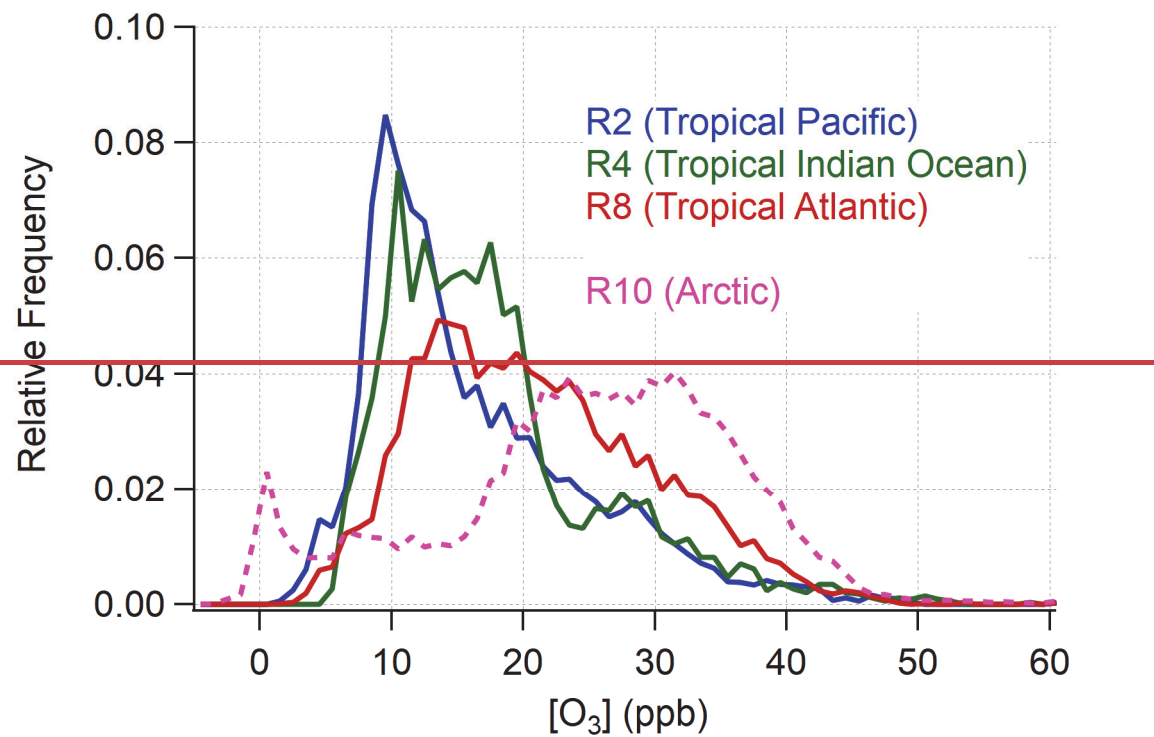
**Figure 5.** Vertical profiles of ozone concentrations by regions, after filtering for LCL72.

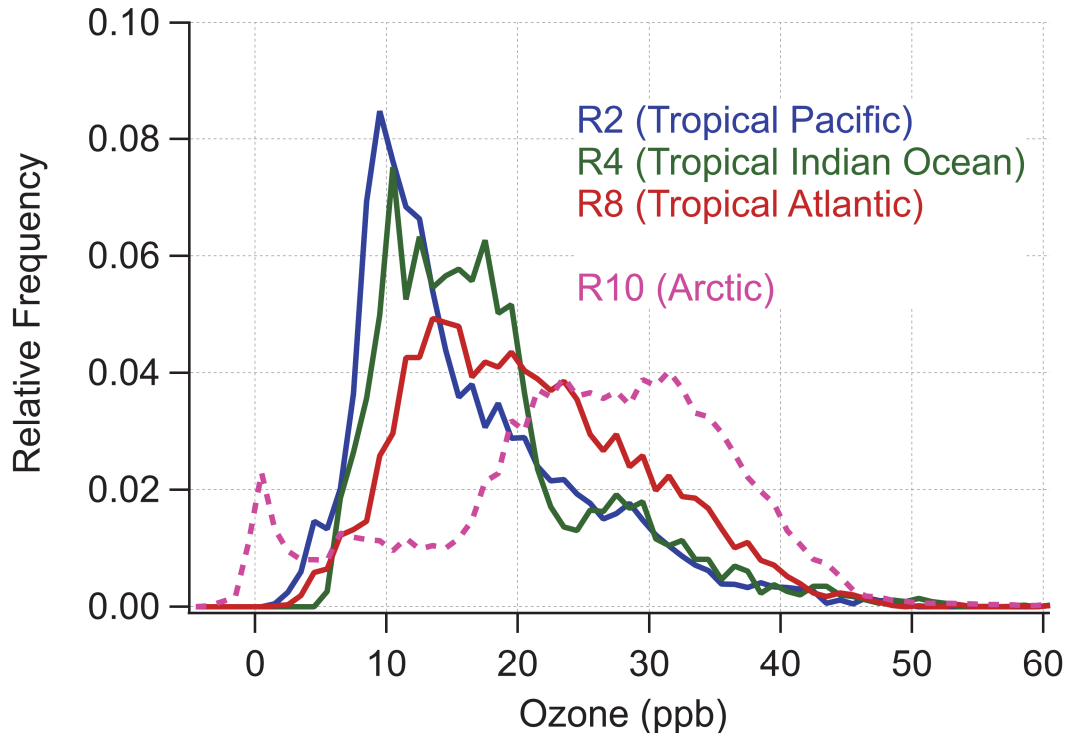
830



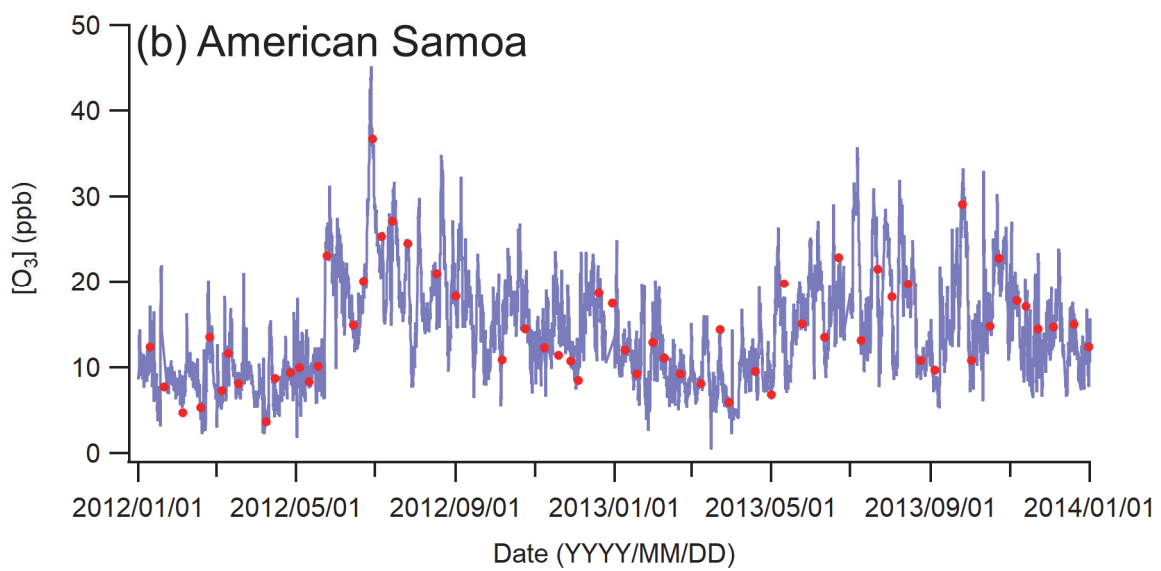
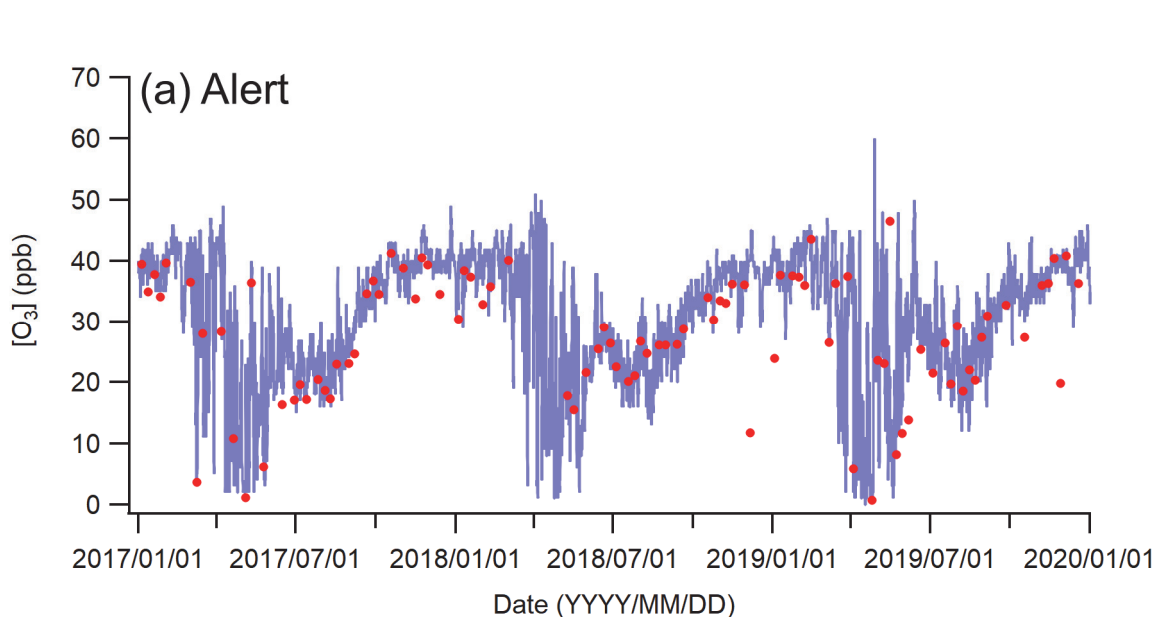


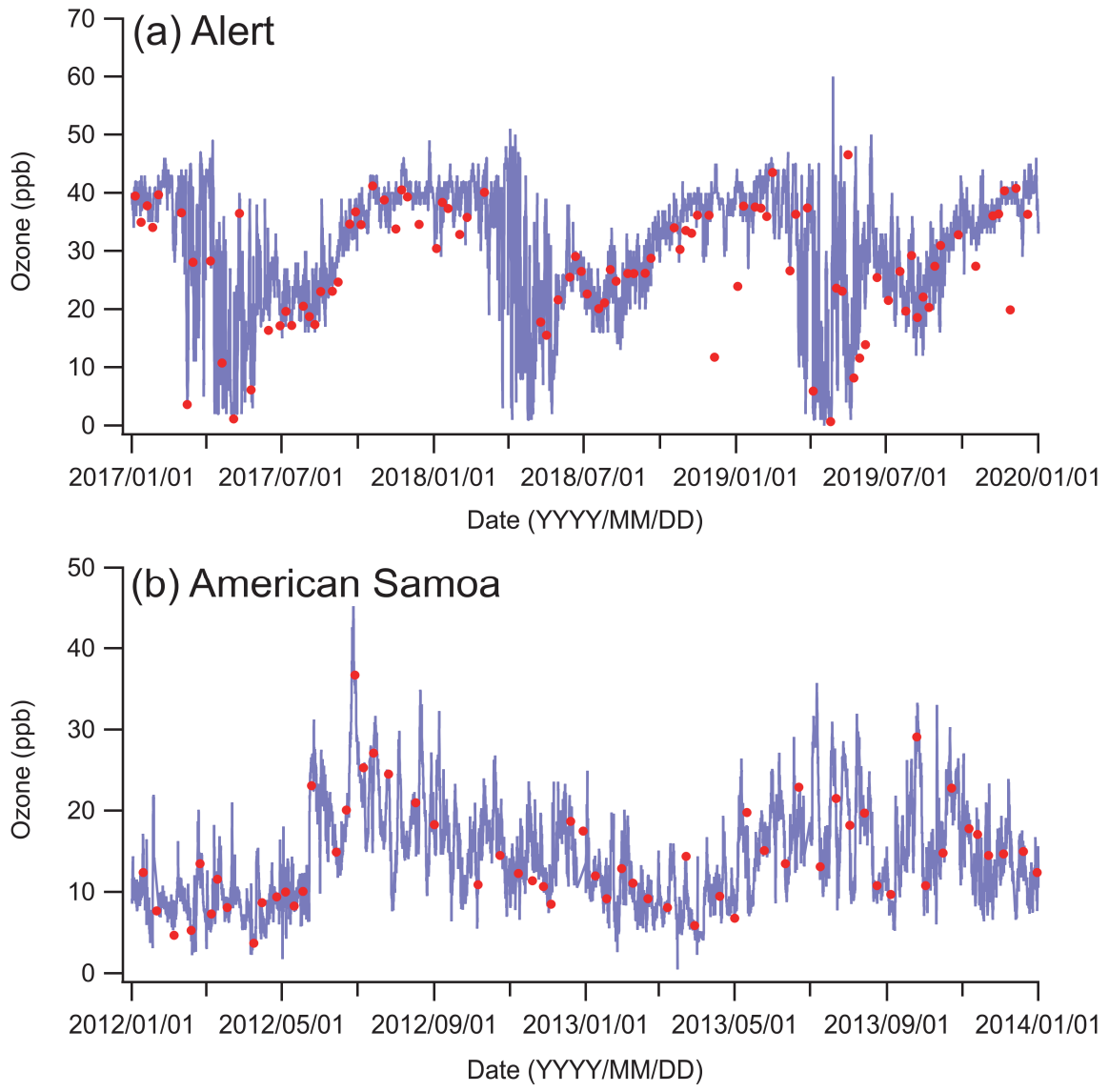
**Figure 6.** Hourly median (thick lines) and interquartile levels (thin lines) and their diurnal variation by regions. (a) R1 and R7 (Pacific and Atlantic northern midlatitudes), (b) R2, R4, and R8 (Pacific, Indian, and Atlantic low latitudes), (c) R3, R5, and 835 R9 (Pacific, Indian, and Atlantic southern midlatitudes), and (d) R10 and R11 (Polar, i.e., Arctic and Antarctic regions). The blue, green, and red line colors correspond to the Pacific, Indian, and Atlantic Oceans.





845 **Figure 7.** Frequency of observed  $\text{O}_3$ -ozone concentrations in 1 ppb bins computed for ship and buoy observations with LCL  
 $\geq 72$  h for tropical regions (Pacific Ocean R2, Indian Ocean R4, and Atlantic Ocean R8) contrasted with the Arctic (R10).





|855 **Figure 8.**  $\text{O}_3$ -Ozone concentrations from surface observations (blue) and the lowest layer of ozonesonde observations (red, ~200 m altitude) at (a) Alert (top panel) and (b) American Samoa (bottom panel).